Bone Reports 16 (2022) 101161

Contents lists available at ScienceDirect

Bone Reports

journal homepage: www.elsevier.com/locate/bonr

Bone hydration: How we can evaluate it, what can it tell us, and is it an effective therapeutic target?

Rachel K. Surowiec [a,b,*], Matthew R. Allen [a,b,c], Joseph M. Wallace [b]

[a] Department of Anatomy, Cell Biology & Physiology, Indiana University School of Medicine, Indianapolis, IN, United States
[b] Department of Biomedical Engineering, Indiana University Purdue University of Indianapolis, Indianapolis, IN, United States
[c] Roudebush Veterans Administration Medical Center, Indianapolis, IN, United States

ARTICLE INFO

Keywords:
Bone water
Skeletal imaging
Bound water
Free water
Structural water
Mechanical properties
Material quality

ABSTRACT

Water constitutes roughly a quarter of the cortical bone by volume yet can greatly influence mechanical properties and tissue quality. There is a growing appreciation for how water can dynamically change due to age, disease, and treatment. A key emerging area related to bone mechanical and tissue properties lies in differentiating the role of water in its four different compartments, including free/pore water, water loosely bound at the collagen/mineral interfaces, water tightly bound within collagen triple helices, and structural water within the mineral. This review summarizes our current knowledge of bone water across the four functional compartments and discusses how alterations in each compartment relate to mechanical changes. It provides an overview on the advent of- and improvements to- imaging and spectroscopic techniques able to probe nano-and molecular scales of bone water. These technical advances have led to an emerging understanding of how bone water changes in various conditions, of which aging, chronic kidney disease, diabetes, osteoporosis, and osteogenesis imperfecta are reviewed. Finally, it summarizes work focused on therapeutically targeting water to improve mechanical properties.

1. Introduction

Bone is a highly heterogeneous composite biomaterial comprised of mineral, collagen, and water. These bone building blocks maintain a complex and dynamic structural hierarchy across discrete length scales that span organ-level, micro-, nano-, and ultrastructural features and molecular structures. Bone can dynamically adapt to local needs at each level of its multi-scale hierarchy, allowing the optimization of its material composition and structure to meet functional requirements. The tissue itself is made up of ~35–45% hydroxyapatite mineral crystals, ~40% organic matrix including type I collagen and other non-collagenous proteins, and ~15–25% water, by volume (Boskey and Robey, 2018). These components combine to provide flexibility, toughness, and elasticity and can change independently, or together, due to aging and disease.

Hydration's essential role in bone across the material's hierarchy has become clear just over the past few decades. Although long accepted that water constitutes roughly a quarter of the cortical bone by volume (Neuman and Neuman, 1958; Robinson, 1952) and can be modulated ex vivo by temperature and solvents (Nyman et al., 2006; Yan et al., 2008), there is now a growing appreciation for how it can dynamically change due to age (Wang et al., 2018), disease (Allen et al., 2015a), and treatment (Gallant et al., 2014). Bulk changes in total water display an inverse relationship with bone mineral content and strength (Elliott and Robinson, 1957; Fernandez-Seara et al., 2004). When water is completely removed, a bone has lower energy to fracture (Evans and Lebow, 1951; Yamada and Evans, 1970), toughness (Evans and Lebow, 1951; Sedlin and Hirsch, 1966) including fracture toughness (Kahler et al., 2003; Nalla et al., 2005), and reduced viscoelastic behavior (Garner et al., 2000; Yamashita et al., 2001), higher hardness (Rho and Pharr, 1999), tensile strength (Dempster and Liddicoat, 1952) and stiffness (Evans, 1973; Rho and Pharr, 1999). Complete dehydration is not physiologically relevant, so understanding how small modulations of hydration, in both directions, and how they influence mechanics is important to understand.

A key emerging area related to bone mechanical and tissue properties lies in differentiating the role of water in its four different compartments, including *free* or *pore water*, water *loosely bound* at the collagen/mineral interfaces, water *tightly bound* within collagen triple helices, and *structural water* within the mineral (Fig. 1). Due to the

* Corresponding author at: 350 N. Blackford St. EL221, Indianapolis, IN 46202, United States.
E-mail address: rksurowi@iu.edu (R.K. Surowiec).

https://doi.org/10.1016/j.bonr.2021.101161
Received 17 November 2021; Received in revised form 10 December 2021; Accepted 11 December 2021
Available online 21 December 2021

advent of- and improvements to- techniques able to probe nano- and molecular scales, our knowledge of these compartments continues to grow from our original understanding (Dempster and Liddicoat, 1952; Evans, 1973), which relied on calorimetry of frozen bone tissue to derive total water (Robinson, 1931). The foundational review of bone hydration conducted by Granke et al. (2015a) set the stage for the bone field to (re)consider hydration's value as a clinical biomarker for bone health and as an attractive therapeutic target in reducing fracture risk (Granke et al., 2015a). The current review will summarize our current knowledge of water across the four identified water compartments and how alterations to each compartment relates to mechanical changes. We also discuss the current state of imaging and spectral techniques used to study bone water. Finally, we summarize how water changes in several disease states (e.g., chronic kidney disease, diabetes, osteogenesis imperfecta, osteoporosis) and how hydration can be therapeutically modulated.

2. Bone hydration – the four functional compartments

2.1. Free water

Water in this compartment can flow freely within pores, vascular canals, central (Haversian/Volkmann) canals, and in the lacunar-canalicular network. It accounts for about 20% of total bone water (Biswas et al., 2012). The literature uses “free” and “pore” water interchangeably, although the term ‘free’ seems more appropriate since the other compartments all refer to a characteristic of water binding, rather than a physical location within the bone. Mechanically, an increase in free water results in a loss of strength and stiffness with a small contribution to a loss in toughness (Fig. 2). This is mainly due to the inverse relationship between bone mineral/mass and free water. Early studies using proton-deuteron exchange nuclear magnetic resonance (NMR) determined free water is exchangeable 1:1 with mineral; the more mineral in the system, the less porous the bone and the less free water (Wehrli and Fernandez-Seara, 2005). This underpins using free water as a direct surrogate for cortical porosity. Ultra-short echo time (UTE) magnetic resonance imaging (MRI) can derive a “porosity index” values, using the fraction of bound and free water, which significantly correlates to cortical porosity measured via micro-computed tomography (μCT) ($r^2 > 0.8$, $p < 0.001$) (Rajapakse et al., 2015).

The portion of free water not found within cortical pores is thought to play an important role in transmitting signal from cell to cell via streaming potential (Liu et al., 2019) and/or as measured fluid shear stress by the osteocyte cell walls (Monteiro et al., 2021; Moore et al., 2018; Morrell et al., 2018). In addition, this free water provides vital nourishment (glucose) to the cells (S. Wang et al., 2021b) and participates in transport of solutes from osteocyte-derived signaling molecules enclosed in the lacunar-canalicular system (order of 0.1–1 μm) (L. Wang, 2018).

2.2. Loosely bound water

Bound water associated with mineral and/or collagen accounts for the remainder of bone's total water and can be categorized into three different compartments: loosely bound, tightly bound, and structural. Loosely bound water is located at the interface of the collagen fibril and mineral crystals resides within the organized layer of collagen molecules and mineral crystals (thickness: 0.160 nm without water, ~0.230–0.255 nm with bound water) and can be associated with collagen or mineral molecule (physical adsorption) (Lees, 1981). Loosely bound water, about ~20% of cortical bone's wet weight (Ong et al., 2012), positively correlates with organic matrix density (i.e. collagen, other immobile molecules and tightly bound water) (Cao et al., 2008) and plays an essential role in transferring loads between collagen and mineral by

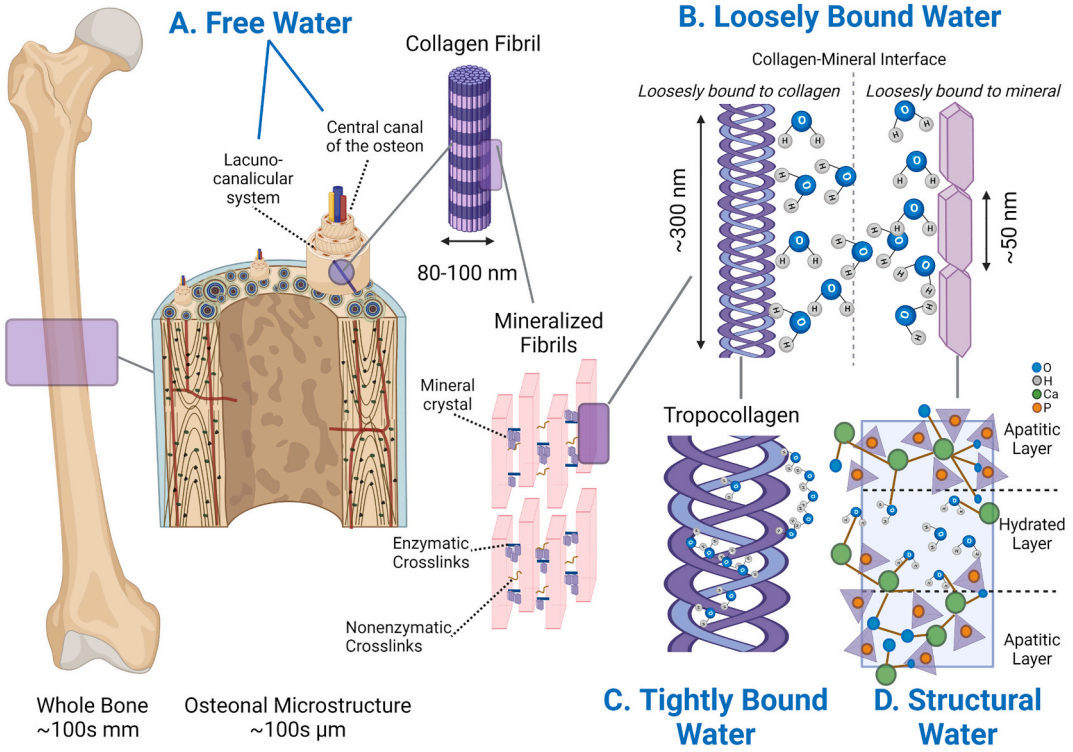

Fig. 1. Bone water is found in four functional compartments. A) Free water is found within central canals and the lacunar-canalicular network. B) Water considered loosely bound is found at the interface of the collagen fibril and mineral crystals and can be associated with/loosely bound to collagen or mineral molecule. C) The tightly bound water fraction is bound to the collagen triple helix forming single and double water bridges, as cleft water within the grooves of the triple helix, and as water contributing to the interfacial monolayer. D) Structural water molecules are found incorporated around the mineral lattice of the carbonated apatite structures forming bridges of hydrogen bonds between ions within the apatite crystal.

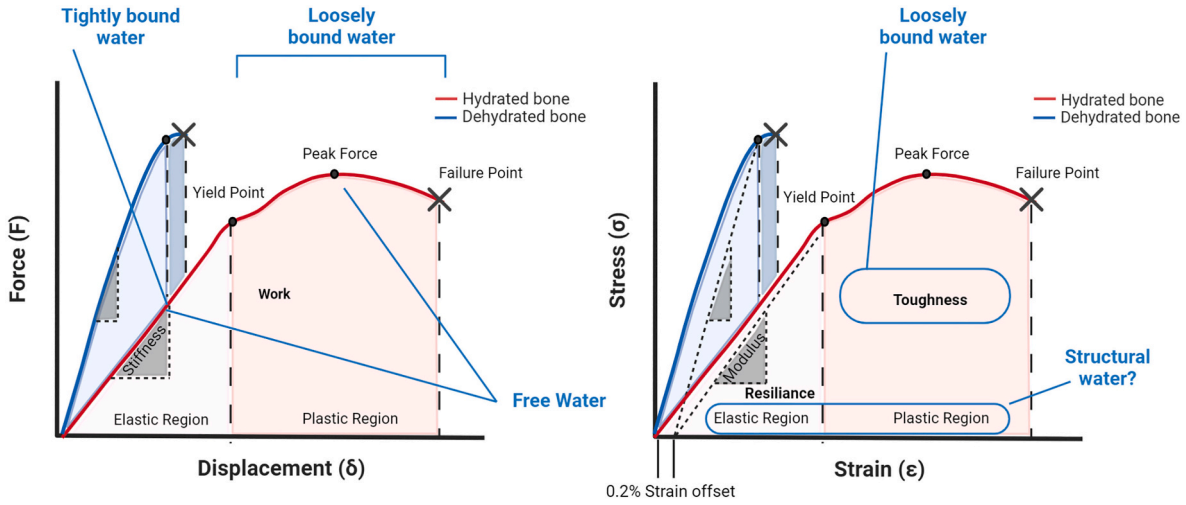

Fig. 2. The four functional water compartments play an integral role in governing bone's mechanical properties. Theoretical force/displacement (A) and stress/strain (B) curves from a fully hydrated and dehydrated bone. A hydrated bone is a ductile material with high toughness and high work. When bone is dehydrated, the material becomes brittle, with high stiffness and modulus and significantly reduced post-yield behavior resulting in decreased toughness and work. While a dehydrated brittle bone can have higher strength (or higher peak/failure force) the lack of water in the system nullifies the plastic region and ductility in the tissue. The four water compartments differentially contribute to bone's mechanical properties. Loosely bound water governs post-yield behavior and increased loosely bound water results in increased toughness while increased tightly bound water decreases stiffness. Increased free water due to increased porosity and can negatively impact both stiffness and strength. Yet free water can also play a role in solute transport thus not all free water is indicative of cortical porosity. Little is known about the role of structural water and its role in governing whole bone mechanical properties. Because of its role in maintaining mineral structure and impacting assembly and aggregation, it likely has properties which govern both the elastic and plastic regions.

allowing sliding at their interfaces. This action reduces shear stresses (Wang and Zhao, 2011) and increases overall tissue toughness (Samuel et al., 2016b). When loosely bound water is removed by thermal dehydration, bone becomes less tough, illustrating its role in governing post-yield mechanical behavior (Fig. 2) (Nyman et al., 2013; Nyman et al., 2006; Yan et al., 2008). The mechanical role of bound water removal under tension and compressive loads at the ultrastructural level has recently been modeled using 2D cohesive finite element analysis. Removal of water under tension reduced nano crack formation, compromised debonding between mineralized collagen fibrils and the extrafibrillar matrix subunits, and hindered crack bridging resulting in brittle failure (Maghsoudi-Ganjeh et al., 2020). In compression, dehydrated bone cannot permit sliding between the mineral crystals in the extrafibrillar matrix and debonding between the extrafibrillar matrix and mineralized collagen fibrils resulting in a stiffer but stronger tissue.

The mineral charge found on the mineral crystal surface was once thought to be the only binding mechanism (Timmins and Wall, 1977) to the highly dielectric water (Marino et al., 1967). Recent work has pointed to the strong hydrophilic properties associated with the neighboring collagen molecules as another factor drawing water to these mineral-collagen spaces. Notably, the role of proteoglycans and their negatively charged glycosaminoglycans (GAGs), which have a great affinity for both collagen and mineral crystals (Best et al., 2008; Hashimoto et al., 1995), has been of interest for their probable role in retaining water in the matrix via their osmotic potential suggesting a coupling effect between proteoglycans and bound water (Wang et al., 2016). When biglycan (*Bgn)*, a highly expressed proteoglycan subtype in bone tissue, is knocked out in mice, total GAGs, bound water, and bone toughness are all significantly degreased compared to wildtype (Hua et al., 2020). When bones from *Bgn* knockout mice undergo full removal of bound water by heat, there is a further reduction in tissue toughness after dehydration indicating the potential involvement of other factors including other proteoglycan subtypes in retaining matrix bound water (Hua et al., 2020). A loss of GAG is associated with loss of bone toughness, a reduction in bound water, a decrease in the amount of Bgn (Wang et al., 2018), and a reduction in plastic energy dissipation in the extrafibrillar matrix (Han et al., 2021; Wang et al., 2016). When wildtype mice are supplemented with chondroitin sulfate (via injection), toughness and matrix bound water increase (Hua et al., 2020), yet the efficacy of oral chondroitin sulfate supplementation in humans remains controversial (Henrotin et al., 2010). Bone glycation reduces bound water fraction (compared to non-glycated bone), suggesting matrix manipulations affect loosely bound water modulation (Nyman et al., 2019).

The portion of loosely bound water bound to/associated with the mineral (Wilson et al., 2005) correlates negatively with elastic modulus and positively to strength (Unal and Akkus, 2015). When mineral-associated loosely bound water is removed by dehydration, loss of creep (rate of deformation under continuous load) is introduced into the system (Eberhardsteiner et al., 2014). This mineral-related fraction of the loosely bound water may contribute to mineral crystal orientation along the length of crystal through interactions with the disordered and highly hydrophilic amorphous calcium phosphate layer (Faingold et al., 2014; Wang et al., 2013) by trapping or binding water forming a hydration shell surrounding the mineral platelets (Von Euw et al., 2018). The water molecules trapped at the amorphous calcium phosphate layer are thought to form hydration spheres serving as “place holders” for the ions to be incorporated into the solid phase (Drouet et al., 2018; Von Euw et al., 2018). It is unknown whether these trapped water molecules contribute to the amorphization of the outer bone mineral itself (Von Euw et al., 2018). The degree of adsorption of water molecules to hydroxyapatite deteriorates with age and disease (Ivanchenko et al., 2017; Welborn, 2021).

2.3. *Tightly bound water*

The water fraction that is tightly bound to the collagen triple helix is found at amounts of ~0.5 g of water per gram of collagen (Privalov, 1958) and is positively associated with bone toughness and negatively with stiffness (Nyman et al., 2006). The long fibrillar collagen structure can hold abundant water due to its shape (large surface area with high water affinity), yet it has been postulated that collagen is fibrillar because the bound water provides structure throughout this length. This is due to the observation that collagen type I structure will shorten upon

water removal (Masic et al., 2015). Within the tightly bound water pool, three distinct collagen-associated water compartments have been identified: single and double water bridges (between alpha helices too distant for direct hydrogen bonding), cleft water within the grooves of the triple helix, and water of the interfacial monolayer (Bella et al., 1995; Brodsky and Persikov, 2005; Lazarev et al., 1992; Wilson et al., 2005). Water also determines collagen's efficient functioning at temperatures (Trebacz and Wojtowicz, 2005): dry proteins cannot unfold upon heating or cooling thus the ability to denature due to temperature is likely caused by the presence of bound water in the system.

2.4. Structural water

Structural water molecules are incorporated around the mineral lattice of the carbonated apatite structures themselves (Von Euw et al., 2018; Yoder et al., 2012). As its name suggests, structural water provides mechanical stability via bridges of hydrogen bonds between ions in the apatite crystal (Wilson et al., 2005). This structural water acts as part of a bridge for the octacalcium phosphate citrate complex (Davies et al., 2014) organizing the mineral platelets (Y. Wang et al., 2013) while providing stability to the inherent crystal imperfections by filling vacancies (Wilson et al., 2005). This mineral-mineral support is crucial because nearly 30% (Alexander et al., 2012) - 70% (McNally et al., 2012) of mineral structures are not in direct contact with collagen fibrils and thus the collagen fibrils themselves cannot serve as a template for organization. It is suggested that structural water provides a medium that allows mineral platelets to maintain organization and create a "continuous cross-fibrillar phase" within the winding volume between disordered collagen fibrils (Reznikov et al., 2018; Von Euw et al., 2018). Structural water may serve a role in regulating the accumulation or aggregation of mineral (Duer and Veis, 2013).

2.5. Distinguishing water compartments by heat or solvents

Thermal and solvent dehydration techniques provide an essential method to study individual bone water compartments ex vivo. Thermal dehydration is performed using a laboratory oven which can maintain a constant vacuum. Temperatures between 21 °C–40 °C, which are below the denaturation temperature of collagen, for durations up to 72 h can be used to remove the free water fraction (Unal et al., 2014). Loosely bound water removal can be achieved by increasing the temperature to 100 °C for 12–24 h (Mkukuma et al., 2005; Mkukuma et al., 2004). Tightly bound water requires temperature in the range of 200 °C for up to 12 h for removal while structural water trapped in the mineral can only be removed after complete decomposition of the organic matrix is achieved typically at temperatures 340–540 °C (Mkukuma et al., 2005; Mkukuma et al., 2004).

Solvents, which exchange water molecules without disrupting collagen's hydrogen-hydrogen bonds, include ethanol (using ascending concentrations), methanol, and acetones (Ferguson, 2009; Nalla et al., 2005; Pathak et al., 2011). Complete exchange with water using solvents may not be achievable because of molecular size of the solvents and their hydrogen bonding capability limit which water pools they can exchange with (Samuel et al., 2014). Even so, solvents are a useful method to remove free, loosely bound, and tightly bound water (Pathak et al., 2011) and, because no damage has been imparted to the collagen and mineral structures (compared to thermal approaches), these methods are generally reversible by rehydration. However, saline rehydration must be done with caution as previous work has demonstrated that all mechanical properties do not necessarily return to pre-dehydration states (Vesper et al., 2017). For detailed experimental outcomes, including mechanical behavior following thermal or solvent dehydration, see review by Granke et al. (2015a).

3. Imaging and spectral methods to quantify bone water

Bone's high photoelectric absorption has made ionizing x-ray-based techniques the modality of choice to image the mineral phase of bone since the introduction of bone radiographs by Roentgen in 1895 (Kanis, 2002; Mahesh, 2013). It is well accepted that assessment of mineral (often by measuring bone mineral density (BMD)) is an incomplete index of fragility, accounts for only a fraction of bone strength as detailed in the review by Hernandez and van der Meulen (2017) and may not adequately predict fracture risk (Kanis, 2002; Marshall et al., 1996; Tremollieres et al., 2010). The extremely high resolution achievable by computed tomography (CT) and high-resolution peripheral quantitative CT (HR-pQCT) has allowed for detailed quantification of microstructural features of the mineral phase, including cortical porosity, giving insight into mechanical properties beyond BMD (Boughton et al., 2019). Yet X-ray based techniques come at a price of ionizing radiation which has long-term health concerns (Lin, 2010) and can damage the very tissue we aim to image (Laperre et al., 2011; Williams and Davies, 2006). This limits its application in clinically vulnerable populations (children, cancer patients) and makes acquisition of multiple imaging timepoints less than ideal (Choksi et al., 2018).

NMR spectroscopy and MRI represent the primary methods used to nondestructively study bone hydration (Jerban et al., 2020c; Mroue et al., 2015; Singh et al., 2013). Compelling progress in solid-state NMR (ssNMR) has allowed us to study the direct relationship of bound water to a host of extracellular matrix components. Advancement in MRI technology has permitted spatially resolved quantification of water down to the bound compartment in vivo. In addition, developments using "vibrational spectroscopy" (Raman spectroscopy, near infrared spectral imaging (NIRSI)) and photoacoustic imaging are positively altering the landscape of bone imaging and spectroscopy and continue to increase our understanding of bone's chemical composition and hydration across its discrete length scales.

3.1. Solid-state nuclear magnetic resonance (ssNMR)

NMR spectroscopy is based on the spins of atomic nuclei; when radiofrequency waves are applied to molecules placed in a strong magnetic field, nuclei will resonate at a biologically specific frequency and emit energy, which is collected and converted to NMR spectra as the spins return to equilibrium. NMR has long been used to determine the structure of small molecules and large proteins in solutions. Solid-state (ssNMR) is becoming an increasingly popular technique that can probe the microstructural details of biomaterials such as bone with picometer resolution in the tissue's absolute native state (Fantazzini et al., 2004; Fantazzini et al., 2003; Murray et al., 2013; Ong et al., 2012; Singh et al., 2014). Hardware updates coupled with technological advancement in ultra-fast magic angle spinning (MAS) methods has improved resolution and sensitivity of ssNMR by attenuating the broadening effects of dipolar couplings and chemical shift anisotropy (Brown, 2012; Hodgkinson and Wimperis, 2009), making the direct evaluation of amide regions, collagen, and their associated water molecules a possibility (Mroue et al., 2015). The technique is credited with the discovery of structural water, which had not been determined until ssNMR studies of mineralized tissue were conducted (Casciani, 1971; Wilson et al., 2005, 2006). Numerous ssNMR experiments have efficaciously probed water across all four of its identified phases and are briefly discussed below. It is important to note that bone specimen preparation is vital to the ssNMR experimental approach. Preparation of bone into a powder using chemical/physical treatment should be avoided due to the risk of perturbing internal features and bonds (Rai and Sinha, 2011). Therefore, intact preparation methods, including breaking the bone into larger "chunks" or machining cylindrical rotor-shaped beams, are preferred for conducting ultra-structural studies in the native state (Nikel et al., 2012; Singh et al., 2013).

1D ^{1}H experiments changed the landscape of bone ssNMR (Granke

et al., 2015a; Horch et al., 2010; Wehrli and Fernandez-Seara, 2005). 1D ^{1}H acquisitions are the cornerstone of deriving total bone water content (Horch et al., 2010; Rai et al., 2013), resolving transverse (T_2) time constants (Horch et al., 2011; Ni et al., 2007), deriving a surrogate measure for cortical porosity (Ni et al., 2007; Wang and Ni, 2003), and monitoring diffusion (Wehrli and Fernandez-Seara, 2005) which have been reviewed previously (Granke et al., 2015a). More recently, ^{1}H experiments have been used to provide additional structural detail regarding matrix triglycerides (Mroue et al., 2016) where lipid chains are shown to be significantly and negatively altered as a function of decreasing water content (Tiwari et al., 2020), suggesting water may have an additional role stabilizing matrix triglycerides (Fig. 3). In combination with ^{1}H, ^{13}C chemical shift can detect conformational collagen changes (Mroue et al., 2012; Rai et al., 2015) and have highlighted water's influence on the mobility of amino acid residues in collagen on the periphery of the triple helix (Reichert et al., 2004) and the presence of a hydrogen bonding network between GAGs in the collagen and mineral interface (Zhu et al., 2009a). The ^{13}C[^{31}P] rotational echo double resonance (REDOR) technique can calculate the distance- and amount of bound water between collagen side-chain residues and the inorganic surface. REDOR experiments have demonstrated the distance between collagen and mineral crystal decreases with decreasing hydration (Rai et al., 2013), increasing age (Nikel et al., 2012), and in states of bone loss (Rai et al., 2013). Finally, 2D ^{1}H—^{31}P heteronucleation correlation (HetCor) experiments, based on the distance-dependent heteronuclear dipolar coupling between phosphate and hydrogen, can be used to measure bound water content relative to inorganic content. 2D HetCor was used to document, for the first time, the presence of structural water in three different locations: occupying vacancies within mineral crystal apatite, in the internal portion of the mineral crystal, and at the mineral surface (Wilson et al., 2006). When used in experiments of bone healing, ^{1}H—^{31}P HetCor was able to document the earliest stages of biomineral formation (and associated water changes) including the size and shape of mineral apatite (Vyalikh et al., 2017) and, in preclinical studies HetCor has shown it can differentiate bound water with treatment (Rai et al., 2013). Although a powerful tool, ssNMR has limitations. For instance, NMR and ssNMR cannot be acquired in vivo, and the technique cannot spatially resolve water compartments. Further, ssNMR requires specialized hardware to achieve MAS limiting its widespread use.

3.2. *Magnetic resonance imaging (MRI)*

MRI is a powerful non-invasive, non-destructive technique which continues to gain interest in bone applications for its sensitivity to biochemical composition and its rich dynamic range. The premise of MRI was born from the basic principle of NMR; (typically) MRI is used to detect ^{1}H nuclei from the water molecules present in a tissue. A radio-frequency pulse (RF) is applied, the protons are stimulated, spin out of equilibrium and, when the RF pulse is removed, return to equilibrium where the energy signal is detected and undergoes a Fourier transform to resolve the image (Mastrogiacomo et al., 2019). MRI is acquired without

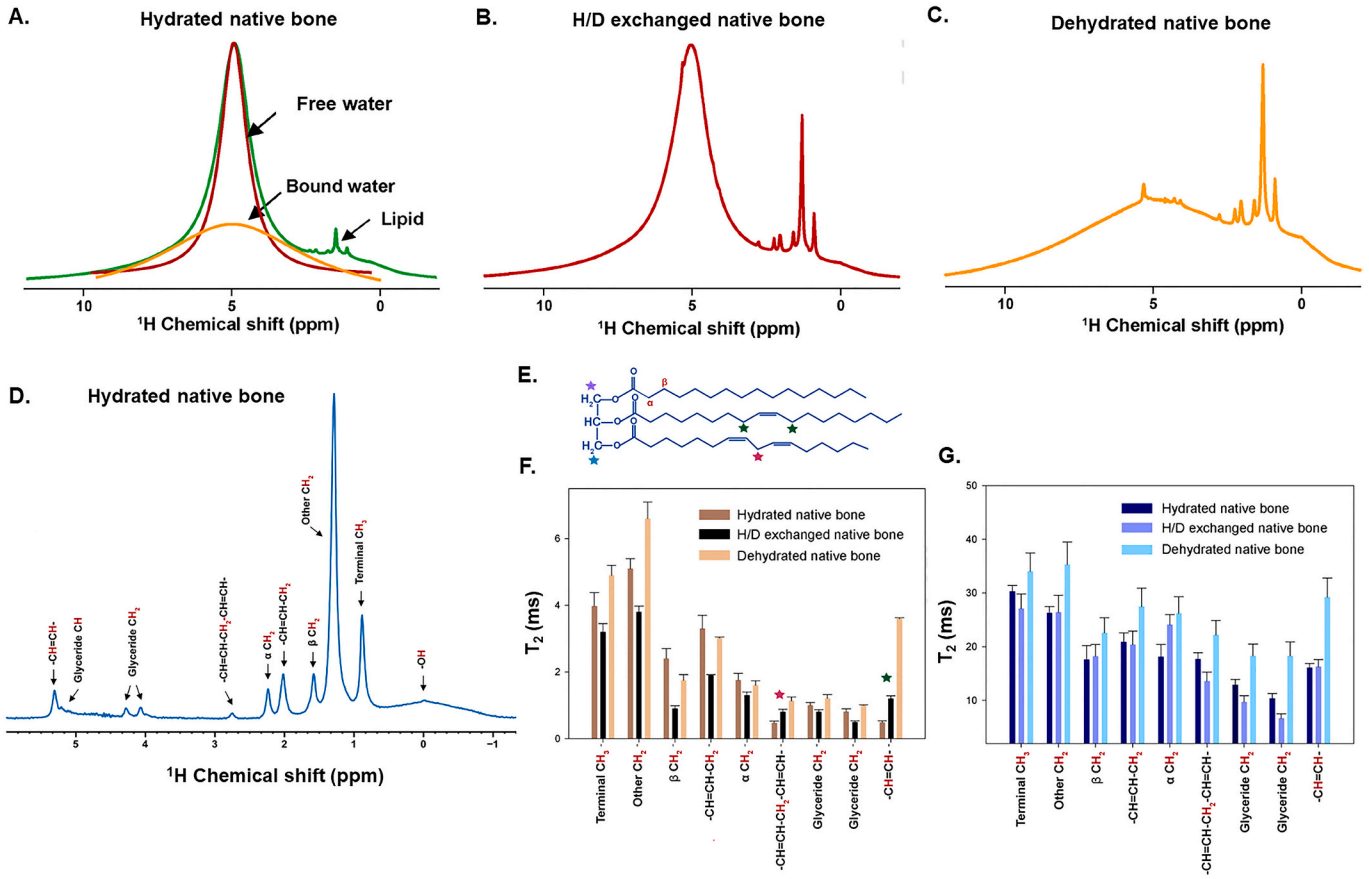

Fig. 3. NMR water measures during dehydration highlight role in stabilizing matrix triglycerides. A) 1H 1D NMR spectra of hydrated native bone (green) showing the distribution of free water (red), bound water (yellow) and lipid peaks. (B) ^{1}H 1D NMR spectra of H/D exchanged native bone and (C) dehydrated native bone. D) ^{1}H 1D Carr-Purcell-Meiboom-Gill NMR spectra (echo time = 2 ms) of hydrated native bone showing assigned spectral peaks of triglycerides. ^{1}H T_2 values from short component resonances (E) and long component resonances (F) of the corresponding triglycerides shown in panel D depict several significant changes to the triglyceride structure under H/D exchange and dehydrated conditions compared to hydrated native bone. Adapted from Tiwari et al. and reprinted with permission (Tiwari et al., 2020).

the use of ionizing radiation, permitting safe longitudinal studies where multiple X-ray based imaging acquisitions would be unfeasible and potentially unsafe (Damilakis et al., 2010). Compared to NMR, MRI can spatially resolve biochemical information and can be acquired in vivo. Yet in conventional MRI, bone appears as a signal void and is unable to capture the tissue's inherently ultra-short transverse relaxation time (T_2) which is dictated by bone's limited hydrogen pool. This is because echo times (TE), or the time between RF excitation and signal acquisition, are too long (a few milliseconds or longer) and most protons from bone's limited water compartments have relaxed before signal is acquired (Horch et al., 2010). More specifically, proton signal intensity is drawn from its water phases with ultra-short T_2 values coming from pore water protons ($T_2 > 1$ ms), loosely bound water protons ($T_2 = 300–400$ μs), tightly bound water found in collagen backbone/sidechain ($T_2 < <20$ μs), and structural/mineral water ($T_2 < <10$ μs) (Granke et al., 2015a; Horch et al., 2010; Nyman et al., 2008; Nyman et al., 2006). Remarkable advances, however, have been made to evaluate bone water's inherently short T_2 components including the advent of three different clinically attractive short T_2 sensitive MRI methods: ultrashort echo time (UTE) (Robson and Bydder, 2006; Siriwanarangsun et al., 2016), free induction decay (FID)-projection otherwise known as zero echo time (ZTE) (Hafner, 1994; Madio and Lowe, 1995; Weiger et al., 2011), and SWeep Imaging with Fourier Transformation (SWIFT) (Idiyatullin et al., 2006).

UTE is by far the most widely implemented in this class of sequences and can be found on most clinical MRI scanners streamlining its accessibility including implementation into clinical research (Ma et al., 2020b).The current state of UTE-MRI can detect implicit signal from free water, matrix loosely bound water, and total water with precision, yet the conventional UTE evaluation of tightly bound or structural water have proven difficult due to restrictions in achieving a nominal T_2 associated with tightly-bound water compartments. Therefore, a broader range of techniques are being explored including the development of 3D-UTE Cones imaging combined with magnetization transfer, ZTE, and SWIFT and Multi-band SWIFT (MB-SWIFT) to resolve the tightly bound pools. Direct measures of the structural water fraction via MRI remains challenging, but if achieved, the spatial information regarding structural water concentrations would represent a significant payoff. While MRI continues to move the field forward through its non-invasive in vivo capabilities; compared to CT, proton-based MRI remains limited by the in vivo spatial resolution achievable while maintaining a sufficient signal-to-noise ratio.

3.2.1. *UTE-MRI loosely bound and free water*

Because the T_2 of loosely bound water is nearly ten times shorter than free water, multicomponent UTE-MRI fitting schemes are used to estimate contributions of (but not absolute proton content) loosely bound and free water. Several studies have elucidated that UTE-multicomponent-derived bound water relates to matrix density while free water confers to cortical porosity (Bae et al., 2012a; Fernandez-Seara et al., 2004; Horch et al., 2011; Nyman et al., 2013; Nyman et al., 2008). UTE-MRI-derived free water varies regionally (Fig. 4) (Zhao et al., 2017), has a strong inverse relationship with bending strength and positively correlates to μCT-derived porosity (Bae et al., 2012b; Manhard et al., 2016), while bound water negatively correlates to porosity and ultimate stress (Bae et al., 2012a). Bicomponent T_2 fitting analysis can detect bone porosities below ranges detectible by μCT and correlates with histomorphometric porosity measures (Jerban et al., 2019b). However, bicomponent schemes can become less sensitive at high field strengths (7 T) (Seifert et al., 2015). Tricomponent fitting schemes using UTE acquisitions have been introduced which eliminate contribution of fat chemical shift to improve upon estimations of loosely bound and free water (Jerban et al., 2020a; Li et al., 2015; Lu et al., 2019). Using human donor bone cortical strips, higher correlations of tricomponent vs. bicomponent bound and free water were found between microstructural (μCT) and mechanical properties (via 4 point bending test) (Jerban et al., 2020a) and tricomponent fitting reduced bound water

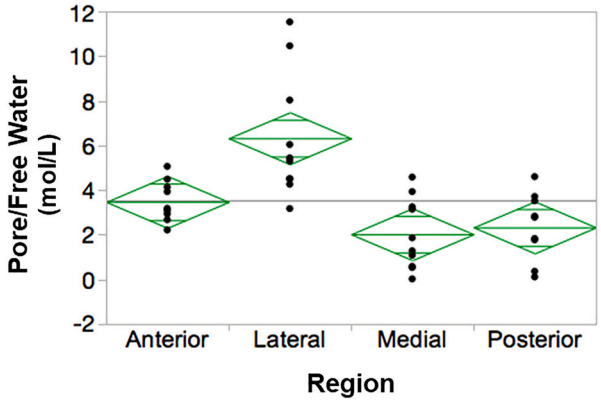

Fig. 4. The amount of free water is regionally dependent. The left tibia from n = 10 healthy volunteers (49 ± 15 yrs) underwent UTE-MRI at 3 T and the cortices were divided into four quadrants (anterior, lateral, medial, posterior) for analysis. Pore water and total water (not shown) was significantly higher in the lateral region compared to the other three quadrants demonstrating regional dependence. $P < 0.001$ via ANOVA followed by post-hoc analysis. Open-sourced figure from Zhao et al. (2017).

overestimation which occurs near the endosteal surface (Lu et al., 2019). All multicomponent T_2 fitting (analysis) requires collecting a series of echo times, the more echo times the better the exponential fit. Thus, scanning times for these studies can become lengthy (≫10–45 min). More recently, direct UTE measures of loosely bound and free water have been obtained though technology advancement. Bound water can be directly imaged using an adiabatic inversion recovery UTE (IR-UTE) which nulls the signal from the long T_2 components (Horch et al., 2012). Conversely, a direct measure of pore water is possible using double adiabatic full passage pulse UTE which uses a preparation pulse to saturate signal from bound water (making it null) followed by a UTE acquisition (Manhard et al., 2015). Both the IR-UTE and double adiabatic full passage pulse UTE can be acquired using most clinical scanners. Choosing an appropriate minimum TE when evaluating bound water is critical to prevent loss of signal from the bound pools; for example, a TE of 50 μs will result in a 1% signal loss of the free water component and a 14% signal loss from the bound water phase (Chang et al., 2015b; Seifert and Wehrli, 2016). This highlights that accurate evaluation of bone water protons by MRI requires an understanding of the biologically different relaxation times within the cortical bone across species, age, and disease, the use of an appropriate phantom, and an understanding of coil sensitivity and radiofrequency pulse durations, flip angles, and inhomogeneity of the system (Du et al., 2010; Ma et al., 2020a). For more information regarding the technical aspects of UTE and the current state of UTE imaging as it relates to bone, the reader is referred to the thorough review by Ma et al. (2020a).

3.2.2. *MRI-derived porosity index*

A singular dual-echo 3D UTE acquisition can be used to calculate the porosity index, a surrogate of cortical porosity based on the measure of free water (the signal ratio between a short (<50 μs) and longer (~2000 μs) TE acquisition). To obtain porosity index, the first echo is acquired using a TE which can capture signal associated with both loosely bound and pore water (total) and the second echo is at a time which captures only the signal arising from pore water (missing the ultra-short relaxation time of bound water). The UTE MRI-derived porosity index biomarker was first described in 2015 by Rajapakse and colleagues and has demonstrated strong positive correlations to μCT-derived porosity ($r^2 = 0.79$, $p < 0.001$), pore size ($r^2 = 0.81$, $p < 0.001$), and UTE-derived pore water fraction ($r^2 = 0.62$, $p < 0.001$) and negatively to bone density measured via peripheral quantitative computed tomography (pQCT, $r^2 = 0.49$, $p < 0.005$) (Rajapakse et al., 2015). Further, the non-ionizing measure of porosity can be acquired in vivo at clinically relevant field

strength, and the acquisition is fast compared to multicomponent fitting schemes making clinical translation attractive (<10 min) (Fig. 5A) (Jones et al., 2021; Rajapakse et al., 2015). Follow up work has demonstrated that the porosity index is correlated to tibial stress (Chang et al., 2015a) and bone stiffness ($r = -0.82$, $p = 0.0014$ (Jones et al., 2021); $r = -0.79$, $p = 0.002$ (Hong et al., 2019)) (Fig. 5B) . Moreover, porosity index has an inverse relationship to bound water and phosphorous content measured by both MRI and near infrared spectroscopy (Fig. 5C) (Hong et al., 2019; Zhao et al., 2017).

3.2.3. MRI-derived tightly bound water

The direct measure of the collagen backbone protons (tightly bound) in native bone tissue remains challenging using conventional UTE-MRI (due to limitations in achieving a near-zero TE) thus alternative MR sequences have been explored. ZTE approaches can achieve a TE = 0 by turning on the projection gradients prior to radiofrequency excitation using a large bandwidth hard pulse and 3D radial center-out encoding schemes. ZTE can provide higher spatial resolution and improved signal to noise ratio compared to UTE (Weiger et al., 2012) because spatial encoding starts without a delay at the full k-space speed. Yet implementation of ZTE is not always feasible because of hardware constraints required to achieve its acquisition parameters. Nevertheless, ZTE has been used in a proof-of-concept study to derive T_1 relaxation time from collagen-related water pools in mice in vivo. Results report a T_1 of 213 ± 95 ms belonging to collagen-bound water which represented a collagen bound water fraction of 7.4% in the mouse femoral diaphysis (Marcon et al., 2017).

To overcome UTE-MRI's inability to directly measure the T2* associated with water of the collagen backbone at current clinically relevant field strengths, a technique called magnetization transfer (MT) combined with UTE-MRI and UTE-MRI multispoke Cones sequences has been deployed as a method to *indirectly* measure bone's collagen proton phase (Chang et al., 2015a; Ma et al., 2018; Ma et al., 2016). A benefit of this technique is that it can be conducted using most clinical scanners at clinically utilized field strength. To determine the indirect measure of collagen's protons, the macromolecular proton, using a two pool MT technique, a high-power saturated radiofrequency pulse is used to saturate protons primarily of the macromolecular matrix. This saturation magnetization is transferred across the protons from macromolecules to the water protons in the bone which can be detected using UTE-MRI. Using this two-pool method of MT, the 'macromolecular proton fraction' macromolecular relaxation time can be estimated (i.e., the estimate of collagen associated water) (Jerban et al., 2019a). If an additional UTE sequence is acquired to capture total water proton density, an absolute measure of the collagenous matrix density coined 'macromolecular proton density' can be estimated from the MT-UTE macromolecular proton fraction and the conventional UTE total water fraction (Jerban et al., 2019a). The macromolecular proton density can be acquired in vivo and is shown to decrease with age in volunteers (Fig. 6A,B). When captured ex vivo, the macromolecular proton density of donor femora showed strong, significant correlation with female donor age ($r = -0.91$, $p = 0.03$) and moderate to strong correlations with μCT-derived cortical porosity and BMD ($r = -0.67$, $p < 0.01$ and $r = 0.65$, $p < 0.01$, respectively) (Fig. 6C). It is assumed this measure represents bone collagenous matrix spatial distribution and could be used to localize or "map" injury or mechanically weak spots in the matrix such as in bone stress injury (Jerban et al., 2018), but work to validate this against spectral techniques (composition) and mechanical outcomes will need to be performed.

3.3. Vibrational spectroscopy techniques

3.3.1. Raman spectroscopy

Raman spectroscopy is a non-destructive spectroscopic technique which relies on elastic scattering of photons (Rayleigh scattering) to detect vibrational and rotational states, chemical structure, and phase in biological systems (Jones et al., 2019). Raman has proven efficacious probing the biochemical composition of bone including the spectroscopic observation of mineral phosphate, carbonate, and matrix collagen (Bergholt et al., 2019; Morris and Mandair, 2011), their mechanical relationships (Makowski et al., 2017), and even matrix lipids and phospholipids (Penel et al., 2005). Raman permits the use of fresh tissue

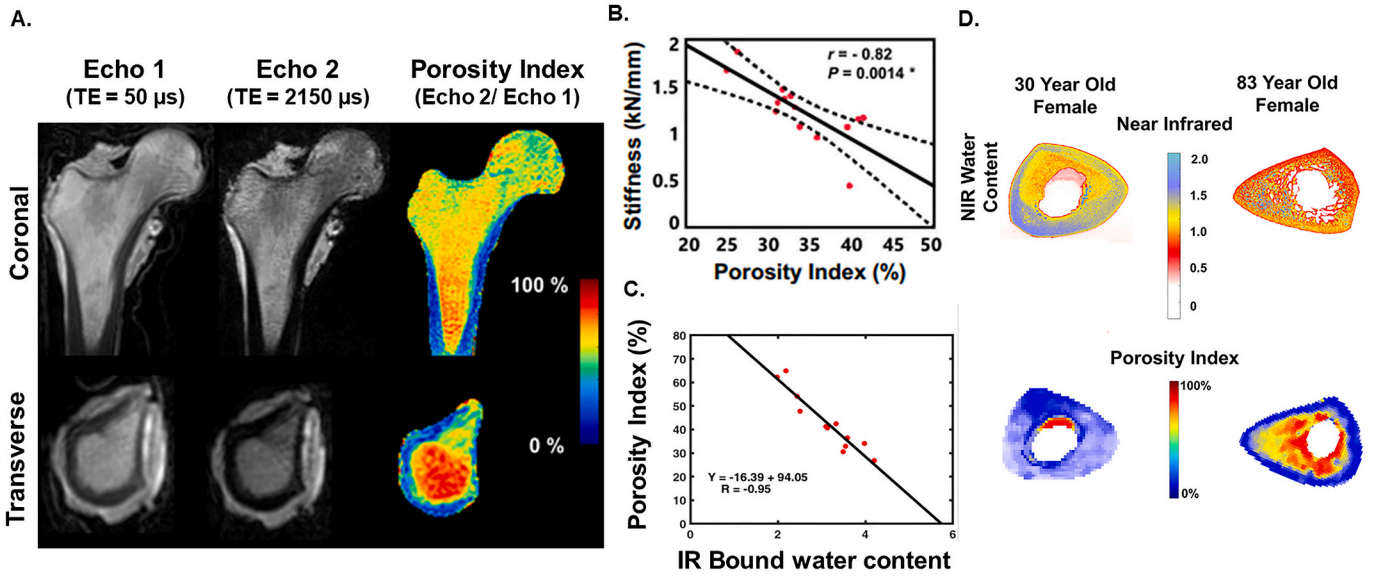

Fig. 5. UTE MRI-derived porosity index correlates to compositional and mechanical properties. A) Coronal (top) and transverse (bottom) views at the same slice location in the proximal cortical shaft of a human cadaveric femora specimen scanned on a clinical 3 T scanner using a dual-echo UTE-MRI sequence. Echo 1 should ideally be acquired at the lowest possible TE to capture only bound water pools. The percent porosity index is computed by taking the intensity of Echo 2 divided by the intensity of Echo 1. B) Femora were subject to mechanical testing to mimic a sideways fall and porosity index (%) was significantly correlated with whole bone stiffness. Error clouds indicate 95% Confidence Intervals. Panel A and B adapted with permission from Jones et al. (2021). C) Porosity index was significantly correlated to bound water measured using near infrared spectroscopy imaging (NRISI). D) Example of NIRSI collagen, water, and porosity index colormaps for two cadavers. The first column is a 30-year-old female, and the second column is an 83-year-old female. Significant degradation of the endosteum can be seen in each scan of the older cadaver. Panel C and D adapted with permission from Hong et al. (2019).

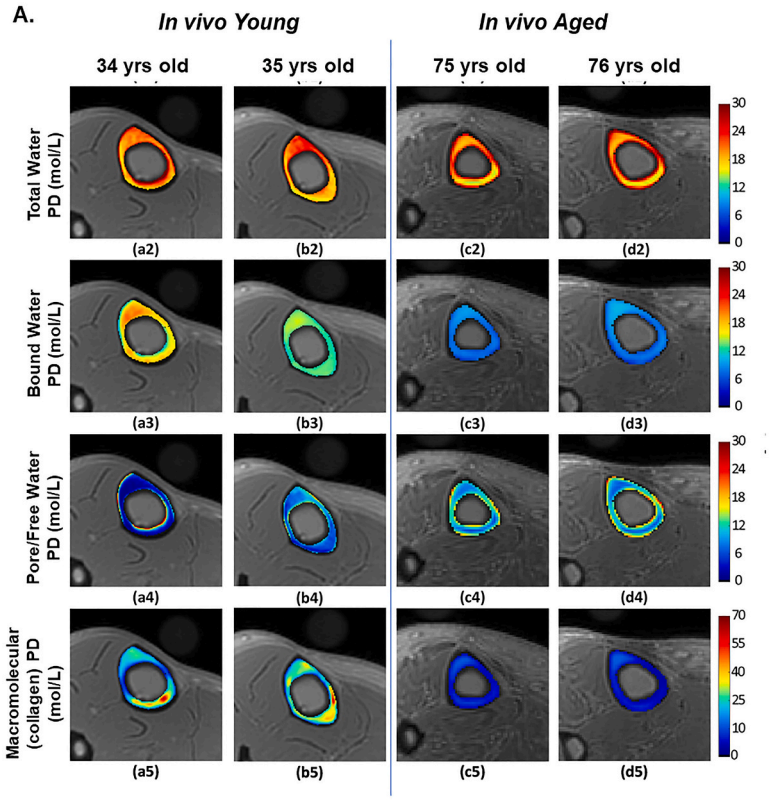

B.

	TWPD (mol/L)	BWPD (mol/L)	PWPD (mol/L)	MMPD (mol/L)
In vivo Young	29.3 ± 6.3	14.8 ± 2.2	14.8 ± 5.3	45.8 ± 12.4
In vivo Aged	36.4 ± 8.3	13.0 ± 1.7	23.4 ± 8.7	29.8 ± 14.8

TWPD, BWPD, PWPD, and MMPD: total water, bound water, pore/free water, and macromolecular proton density, respectively

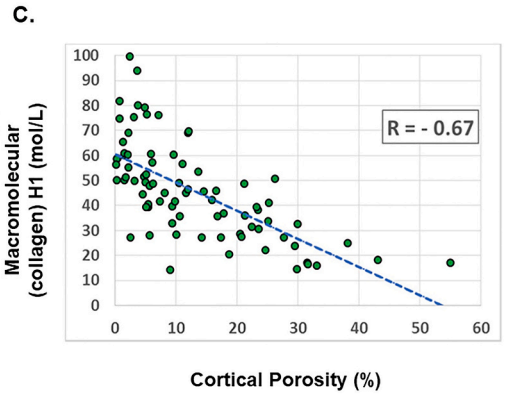

Fig. 6. 3D UTE Cones MRI can detect bound, free and collagen water in vivo. A) Generated proton density maps showing total water, bound water, pore/free and macromolecular (collagen) proton densities from two young volunteers (34 yrs., a2-a5 and 35 yrs., b2-b5) and two aged volunteers (75 yrs., c2-c5 and 76 yrs., d2-d5). B) Corresponding average proton densities from in vivo acquisitions (ten young healthy 34 ± 3 yrs. and five aged women 78 ± 6 yrs). C) Scatter plot and linear regression analyses of the macromolecular proton density and μCT-derived cortical porosity. Analysis was performed on using ex vivo acquisitions from eight donor specimens (63 ± 19 years old, 5 women, 3 men). Images adapted from Jerban et al. with permission (Jerban et al., 2019a).

(in addition to fixed and embedded tissue), and tissue that has been stained or fluorescently labeled (allowing for analysis during period of treatment/rapid bone growth) (Donnelly et al., 2010). Commercial Raman systems lack the sensitivity to resolve the OH-stretch band range, so custom short-wave infrared (SWIR) systems have been designed to achieve the sensitivity necessary to identify both water compartments and to which molecule they are bound to (Unal et al., 2014). Using the SWIR technology, four OH-stretch band peaks have been identified through dehydration experimentation including: collagen related water at peak 3220 cm^{-1}, NH groups (collagen backbone) and their related water at peak 3325 cm^{-1}, water associated with OH of hydroxyproline next to collagen water at 3453 cm^{-1}, and mineral-mineral (OH) water at 3584 cm^{-1} (Fig. 7A) (Unal et al., 2014). Based on the rate these four peaks were replaced by deuterium oxide, Unal et al. defined four spectroscopic biomarkers: I_{3220}/I_{2949}, I_{3325}/I_{2949} and I_{3453}/I_{2949} reflecting collagen-related water phases and collagen portion of bone while I_{3584}/I_{2949} reflects mineral-related water and the mineral portion of bone. Using serial Raman collections throughout dehydration, the authors observed Raman collagen-associated water (I_{3220}/I_{2949} and I_{3325}/I_{2949}) positively correlated with toughness ($r^2 = 0.81$ and $r^2 = 0.79$, both $p < 0.001$) and post-yield toughness ($r^2 = 0.65$ and $r^2 = 0.73$, both $p < 0.001$) while mineral related water (I_{3584}/I_{2949}) positively conferred to strength ($r^2 = 0.46$, $p < 0.001$) and negatively to elastic modulus ($r^2 = 0.78$, $p < 0.001$) via 3 point bending test (Fig. 7B–E) (Unal and Akkus, 2015). Work by others reported that an increase in loosely bound water is observed with a concurrent increase in Amide *I* subpeak ratio which is related to collagen I's helical structure (Nyman et al., 2019). This observation highlights the strength of Raman-based measures by providing spectral information about the moieties where molecules attach.

3.3.2. *Near-infrared spectral imaging (NIRSI)*

NIRSI is a fast spectral technique which measures signals from molecular vibrations following incident radiation of the sample. For bone, NIRSI is particularly proficient at imaging organic components such as collagen and fat content as well as the spatial distribution of water (Chang et al., 2017). For preparation of the sample, NIRSI is non-destructive and can measure intact samples with limited or no preparation including no chemical reagents (Rajapakse et al., 2017) which contrasts with other traditional methods of biochemical analysis. Another benefit of NIRSI is its ability to image at high frequencies which allows for greater depth penetration (on the order of mm to cm) which makes it optimal for probing bone's cortex. NIR water absorbances included three currently identified peaks at 5152, 6560 and 7008 cm^{-1} (Ramyasri Ailavajhala et al., 2019). NIRSI can provide additional, direct measures of matrix components such as collagen in addition to water. NIRSI collagen matrix (4608 cm^{-1}) peak correlated to NRISI water peak (7008 cm^{-1}) ($r = 0.69$, $p = 0.004$) and NIRSI water peaks at 5152 and 7008 cm^{-1} correlated to free and bound water derived from UTE (free: $r = 0.735$, $p = 0.016$ and bound: $r = 0.71$, $p = 0.01$) (Rajapakse et al., 2017). One challenge in evaluating water content using spectral techniques is the risk of dehydration, or even rehydration due to atmospheric humidity, occurring during data acquisition hindering interpretation and reproducibility among other things. Ailavajhala et al. describe the application of an environmentally controlled chamber for NIRSI to increase repeatability of water measures in the bone without the influence of atmospheric moisture (Ailavajhala et al., 2019). Using NIRSI collected in cortical bone at size different lyophilization time points, they were able to use a partial least squares model to generate a water calibration curve (in good agreement with gravimetric assessment). They reported peak 6560 cm^{-1} became insignificant following 48 h of dehydration and

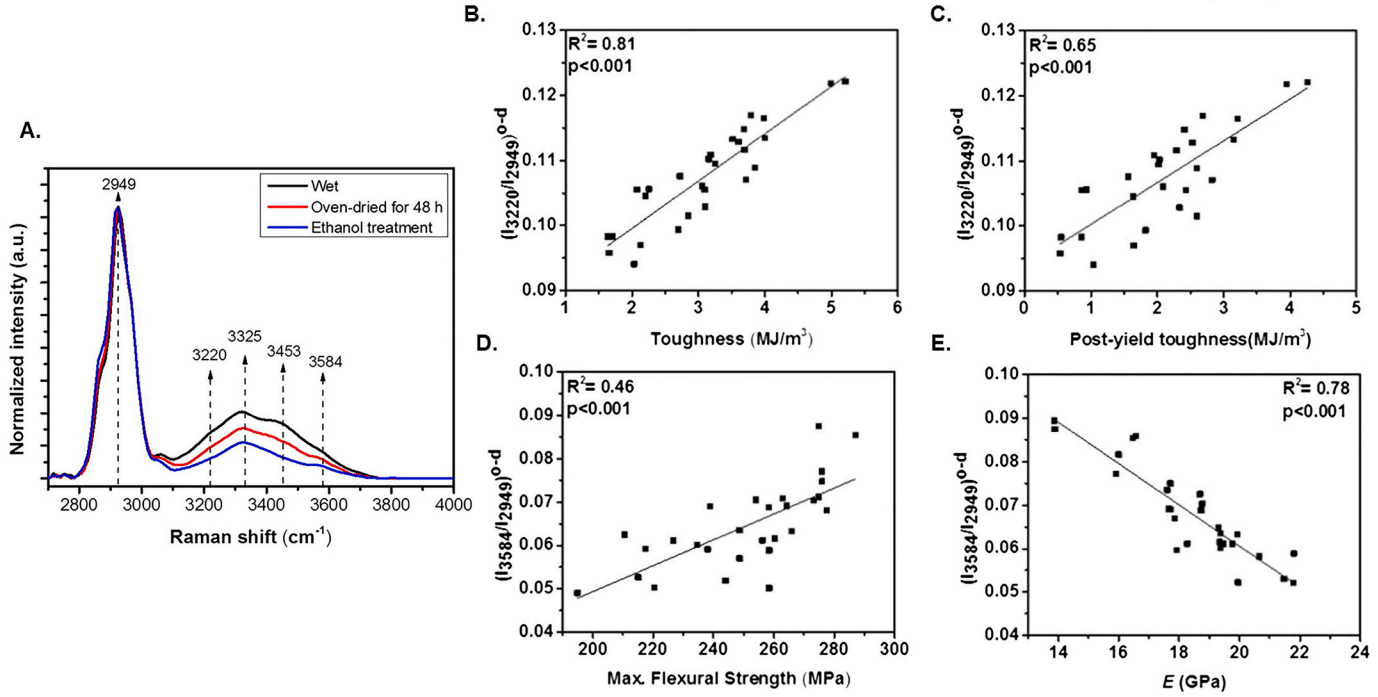

Fig. 7. Raman collagen- and mineral- related water measures correlate with bone mechanical properties. A) Average Raman intensity changes of bone during sequential dehydration in an oven for 48 h followed by ethanol treatment. There was a gradual decline in the Raman intensities of bone's OH-stretch band during sequential drying. Every spectral trace provided in this figure is the average of 90 spectra. Spectra are normalized with respect to the CH-stretch intensity that is representing the amount of protein in bone. R^2 pairwise correlations between mechanical properties (3-point bending) and Raman spectroscopic bone water biomarkers obtained from oven-dried bone samples. Significant correlations exist between collagen associated water (B) (I_{3220}/I_{2949}) o-d and toughness and (C) (I_{3220}/I_{2949}) o-d and post-yield toughness. Mineral associated water was significantly correlated (D) (I_{3584}/I_{2949}) o-d and maximum flexural strength, and (E) (I_{3584}/I_{2949}) o-d and the modulus. Reprinted with permission from Unal and Akkus (2015).

any remaining water absorbances were likely to reflect tightly bound water (Ailavajhala et al., 2019) but more work needs to be conducted to validate this observation.

3.4. Photoacoustic (PA) imaging

PA imaging detects the acoustic signal triggered by infrared light irradiation to provide high-resolution optical images giving way to parameters such as molecular content depth and absorption coefficients (Xia et al., 2014). Specifically, the pulsed infrared light is absorbed by the biological material which generates ultrasound waves on the principle of thermoelastic expansion. These ultrasound waves are collected by an ultrasound transducer and 3D images of optical absorption contrast are derived (Beard, 2011). Those tissues considered "optical absorbers" such as blood and bone water are ideal for PA imaging where PA imaging can overcome limitations when using ultrasound alone (where the collected signal is reflected from the tissue layers and limits the achievable penetration depth). PA imaging can be acquired in situ, ex vivo, and in vivo (Park et al., 2020) although in situ and ex vivo is often optimal due to competing signal with surrounding blood flow. The molecular vibrational state of water is affected based on whether it is bound or unbound in a tissue. Since water can absorb electromagnetic waves found within the radio frequency and microwave spectra, it is a powerful absorber using radio frequency-based PA (otherwise referred to as thermoacoustic PA). More recently, work has demonstrated the potential of a near-IR based PA imaging to detect water spectra (Xu et al., 2010) using a light source, but thermoacoustic PA remains the primary technique in bone thus far. In bone applications, PA imaging has been performed to obtain chemical information from the mineral, collagen, lipid, oxygenated and deoxygenated hemoglobin, and has even described a PA-derived BMD measure in good agreement with BMD measured using conventional approaches (Feng et al., 2021; Feng et al., 2015; Feng et al., 2020; Lashkari and Mandelis, 2014). Recent work used PA imaging to characterize absorption frequency from water, collagen, and lipids in osteoporotic and control rabbit bone. Using the relative content, PA demonstrated significantly decreased collagen, increased lipid, and no change for relative water content between osteoporosis and control groups (Feng et al., 2021). While there were no significant changes to water between groups, data presented the feasibility of PA imaging to derive water in bone for the first time. Initial results are promising as PA is a low-cost, non-ionizing and patient-friendly method that can provide information regarding the organic and nonorganic bone tissue and may prove to be a method that can provide a more "complete" picture of bone health.

4. Bone water with age and disease

BMD almost universally falls short across disease state in predicting fracture risk and fracture resistance. Therefore, a biomarker such as bone hydration, that can predict additional aspects of bone health, represents a potential clinical tool that could complement BMD in assessing bone disease and treatment efficacy. Work has been conducted characterizing bound and free water in aged and osteoporotic bone, including correlating how free water relates to cortical porosity. More recently, studies have applied UTE-MRI, ssNMR, NIRSI, and Raman spectral techniques to understand how alterations in hydration with aging and diseases such as chronic kidney disease, diabetes, and osteogenesis imperfecta relate to mechanical outcomes.

4.1. Aging

Fracture risk increases in the aging skeleton; nearly 50% of women and 25% of men will sustain a fracture after 50 years of age (Sheer et al., 2020). When an aged bone fails, the fracture is characterized by a

reduced strain at failure and a more linear crack pattern that has reduced crack-initiation toughness and crack-growth toughness (Katsamenis et al., 2015; Koester et al., 2011; Nyman et al., 2013; Ritchie et al., 2006). Historically, reduced bone strength was thought to result from lower bone mass, density, and alterations to skeletal architecture. These factors can only explain ~75% of increased fracture risk due to age, and increased fragility is often observed with a disproportionate loss in mass, trabecular reorganization, or decreased BMD (Burr and Turner, 1999; Hui et al., 1988; Kanis et al., 2001). Recent work has illuminated age-related changes in bone water within the extracellular matrix including increased free water, decreased bound, and alterations to the water residing on the collagen backbone.

Total water under normative conditions can range between 10 and 20% of total cortical volume and drop to 5% by the 6th decade of life (Neuman and Neuman, 1958; Robinson, 1952). Total water proton density measured via UTE-MRI correlates significantly with BMD ($r = 0.71$, $p < 0.01$) in aged human donor samples (61 ± 24 yrs. old) (Jerban et al., 2020b). However, relying on bulk water to predict fracture risk in the aged skeleton is likely insufficient. Horch et al. demonstrated that free water had strong negative correlations and bound water strong positive correlations with peak stress while bulk water did not correlate with the measure (Horch et al., 2011). Numerous MRI-based studies indicate that free water increases with aging, and MRI-derived free water positively correlates with μCT-derived cortical porosity (Akbari et al., 2016; Rajapakse et al., 2015; Rajapakse et al., 2017; Wehrli and Fernandez-Seara, 2005). The strength of free water as a non-invasive marker of cortical porosity has been exploited in the aging skeleton using the MRI-derived porosity index as a non-ionizing method to track microstructural matrix alteration. In aged specimens, porosity index positively correlates with increased number and size of pores and direct measures of pore water using UTE-MRI and NIRSI (Chang et al., 2015a; Rajapakse et al., 2015). In aged donor specimens (72.1 ± 15.0 yrs. old, ten male, five female), UTE-MRI porosity index measured at the cortical shaft significantly correlated with whole bone stiffness ($r = -0.82$, $p = 0.0014$) calculated using a mechanical test mimicking a sideways fall (Jones et al., 2021). Notably, multiple regression analysis demonstrated that porosity index was a strong predictor of bone stiffness independent of volumetric BMD and cortical thickness indicating its value in predicting whole-bone mechanical integrity. While free water appears to be a viable biomarker in this context, its value largely lies in its ability to predict porosity with less clarity around the specific impact on free water.

Bound water is vital to maintaining bone toughness and strength (Samuel et al., 2016a; Zhu et al., 2009b), both of which are reduced with age (Granke et al., 2015b; Horch et al., 2011; Nyman et al., 2013). Bound water is nearly 40% lower in elderly cadaveric specimens (73 ± 5 yrs) compared to young specimens (26 ± 6 yrs), accounting for upwards of 70% of the age-associated lower bone toughness (Fig. 8A–C) (Wang et al., 2018). Bound water loss and decreased toughness are often seen with collagen derangements suggesting a coadjuvent relationship where changes may be successive or concurrent steps in aging. Advanced age in BALB-c mice (20 mo) is associated with significantly lower femoral toughness, fracture toughness, and matrix bound water (via ^{1}H NMR), and higher enzymatic (mature hyroxylysyl-pyridinoline) and non-enzymatic crosslinking (pentosidine) and Amide *I* sub-peak ratio (via Raman) (Creecy et al., 2020). Increased Amide *I* sub-peak ratio may help explain decreased bound water due to diminished hydrogen bonding sites between residues of collagen and surface mineral crystal. Similar extracellular matrix compositional changes (higher AGEs and cross-linking) and lower bound water were observed alongside lower fracture resistance in aged (24 mo) male Fischer F344 rats (Uppuganti et al., 2016). As a result of these and other works (Bridelli et al., 2017; Jazini et al., 2012), it is hypothesized that loss of bound water and increased glycation are related and consequential steps during aging. While it is not entirely clear, evidence supports a loss of bound water may initiate glycation events (Bridelli et al., 2017) while increased cross-linking may physically displace existing or prevent new bound water (Kopp et al., 1989).

4.2. Osteoporosis

Osteoporosis represents a systemic metabolic skeletal disorder marked by altered bone remodeling leading to reduced bone strength and increased fracture risk (Lorentzon and Cummings, 2015). BMD has long served as a diagnostic measure for osteoporosis where the disease is characterized by a BMD which falls below −2.5 standard deviations for the mean BMD of normal young females (Kanis, 1994). Porosity index in postmenopausal women has been shown to range from 15 to 38% (Rajapakse et al., 2015). More recently, work has been conducted to evaluate relationships between age and body mass index (BMI) among pre- and postmenopausal women. Porosity index (%) measured at the tibia in pre- and postmenopausal female volunteers (45.7 ± 15.9 yrs) using UTE-MRI was positively correlated with age in postmenopausal but not premenopausal women and negatively correlated with BMI in both groups (Chen and Yuan, 2018). These correlations were not observed when porosity index was calculated at the femoral neck, a common fracture site in osteoporosis. Interestingly, porosity index at the tibia and femoral neck were not correlated suggesting important region-dependent alterations to porosity and bone water are present.

In a recent study, Raman spectroscopy was acquired in iliac crest biopsies collected from postmenopausal women who have sustained a fracture and compared to age- and BMD-matched non-fracturing

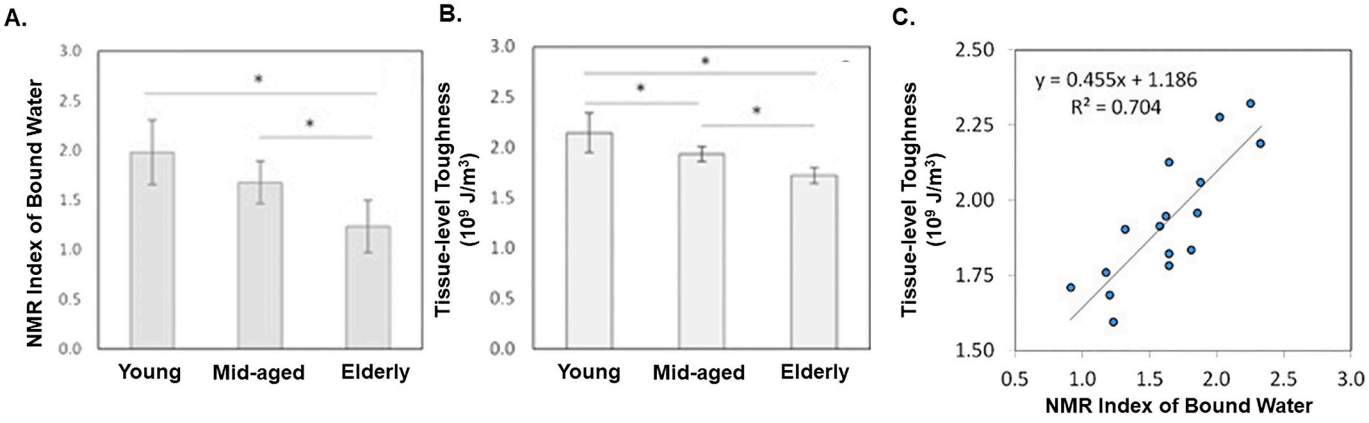

Fig. 8. Aging reduces bound water and tissue-level toughness. A) Age-related effects in the amount of bound water measured via NMR and B) tissue-level toughness via nanoscratch test. Data shown are mean ± SD. n = 6. *p < 0.05. C) Bound water was significantly positively correlated with tissue-level toughness (p < 0.05). Figures adapted from Wang et al. (2018).

postmenopausal women (Rokidi et al., 2019). Women who had sustained an osteoporotic fracture demonstrated significantly decreased tissue water as well as lower GAG, higher pyridinoline (enzymatic collagen cross-link), and higher N(6)- carboxymethyllysine (an AGE). The greatest difference between fractured and non-fracture controls came from the Raman measure of tissue water. Mechanically, these changes result in significantly lower hardness and modulus via nano-indentation (Vennin et al., 2017). Results in this cohort of age- and BMD-matched bone strongly suggest water could serve as an independent determinant of fracture risk. While measures were not derived using in vivo techniques, they were calculated from iliac crest biopsy which is a standard, although invasive, method for obtaining clinical biopsy suggesting further studies could be utilized validating biopsy results with in vivo findings (using UTE-MRI, for example).

Ovariectomized (OVX) animals have long served as a preclinical model to study postmenopausal osteoporosis. Using SWIFT MRI in a cross-sectional study design, cortical bone water signal intensity was significantly higher by 8 weeks post-OVX surgery compared to SHAM controls (Sukenari et al., 2015). MRI-based measures of signal intensity were positively correlated with new bone area measured using histomorphometric analysis, but no correlation was found with BMD. In the only study to date applying in vivo MRI-based measures to follow disease progression, SWIFT-MRI was used to quantify cortical water, cortical matrix T_1 relaxation times (a tissue-specific biomarker where measures are related to tissue organization), and marrow fat content at baseline and 2, 4, 10 and 12 weeks post-OVX (Surowiec et al., 2021). By week 10, SWIFT detected a significant decrease in cortical water and T_1 relaxation times, indicative of a more disorganized matrix with reduced bound water, and a significant increase in marrow fat content consistent with postmenopausal osteoporosis. However, bi- or tri- component analysis was not conducted in either study thus the authors could not distinguish which water compartment(s) were driving OVX-related changes.

4.3. Chronic kidney disease

Kidney injury or disease can catalyze a cascade of biological events involving numerous pathophysiological pathways that have prominent and deleterious effects on the skeleton. CKD patients have a 2–14-fold greater fracture risk than the age-matched healthy population which increases with disease progression (Nickolas et al., 2008). Susceptibility to fracture appears well before the need for dialysis and cannot be fully explained by changes in bone mass and BMD. There is a growing body of pre-clinical literature documenting alterations in matrix tissue properties (collagen, hydration) which are linked to bone brittleness and are also present in CKD (Iwasaki et al., 2015; Mitome et al., 2011; Newman et al., 2014).

The male Cy rat model of progressive CKD has a bone phenotype that includes significantly increased cortical porosity (McNerny et al., 2019) and severely diminished mechanical properties compared to normal littermates (Newman et al., 2014). At the material level, modifications in collagen crosslinking and bone hydration are present and are differentially affected in high- and low-turnover subtypes (driven by parathyroid hormone (PTH)) of the disease (Allen et al., 2015a). Compared to normal littermates, high-turnover (high PTH) CKD rats had cortical bone with lower bound water and higher pore water; low turnover (low PTH) CKD rats had cortical bone with higher bound water and lower pore water (Fig. 9A) (Allen et al., 2015a). Serum PTH correlated positively to pore water and negatively to bound water (Fig. 9B,C). Pore water tracked closely to changes in cortical porosity, which was higher in high-turnover animals and lower in low-turnover animals at 35 weeks. Bound water was observed to be inversely related to mineralization. Notably, at 30-weeks, mineralization was largely unchanged (measured by Raman spectroscopy) in high turnover animals yet bound water fraction (by UTE-MRI) was significantly lower. Because significant changes in cortical porosity were not observed, it is plausible that alterations in bound water at the mineral/collagen interface may

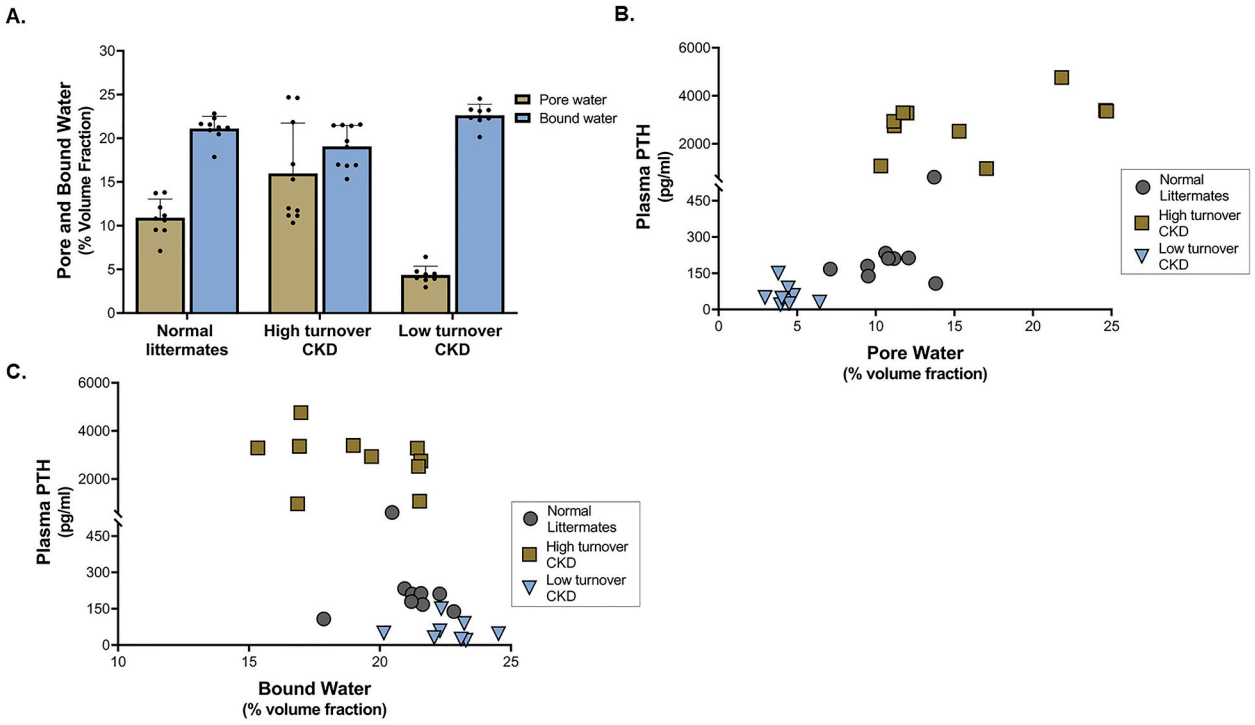

Fig. 9. Matrix hydration is differently impacted in low- vs. high turnover CKD. A) Pore water fraction at the femoral cortex measured via NMR was significantly higher in high turnover CKD and significantly lower in low turnover CKD compared to normal littermates. Bound water fraction was significantly lower in high turnover CKD and higher in low turnover CKD compared to normal littermates. All data presented as mean ± standard deviation. * $p < 0.05$ compared to normal animals. B) Plasma PTH was positively correlated with pore water fraction ($r = 0.81$) and C) negatively correlated with bound water fraction ($r = -0.70$). Figures adapted from Allen et al. (2015a).

preceded changes in bulk mineralization serving as an earlier event or biomarker in the cascade of CKD-associated skeletal derangements.

4.4. Diabetes

Diabetes is a chronic, complex metabolic disorder with wide-reaching clinical manifestations. Under diabetic conditions, patients can have increased fracture risk, delayed fracture healing, and impaired bone formation (Vestergaard, 2007). Diabetic patients typically present with normal or even high BMD coupled with low bone turnover which cannot explain the high rate of facture (Farr and Khosla, 2016). Thus, diabetes represents a paradoxical bone disorder where normative or high BMD is coupled with compromised bone quality leading to poor mechanical outcomes.

Raman-derived tissue water content (based on nanoporosity; calculated from the ratio of integrated spectral slice 494–509 cm^{-1} (PMMA to Amide III) was measured in tetracycline labeled iliac crest biopsies from premenopausal women with Type 2 diabetes (Rokidi et al., 2020). Actively forming cortical bone nearest to the osteon demonstrated the greatest water content which decreased significantly as a function of tissue age determined by tetracycline labels. Biopsies were fixed in ethanol thus analysis of water peaks as described by Unal and Akkus (2015) could not be conducted. Tissue-level assessment in patients with Type 1 diabetes remains limited.

SWIFT MRI (using a TE ~ 0) could detect changes between diabetic and control male Wistar/ST rats two weeks following streptozotocin (STZ) injections to induce T1D, where changes in BMD were not detectable until week eight (Minami et al., 2018). At two weeks post STZ, mechanical properties including stiffness and energy absorption were significantly compromised and bone formation measured via histomorphometry was suppressed. Proton-based MRI-SWIFT measures, which could detect diabetic-induced bone changes in the matrix four week prior to changes in BMD by μCT, suggest matrix water is altered before bulk mineral manifestations are detected.

4.5. Osteogenesis imperfecta

Osteogenesis imperfecta (OI) is a rare and severe heritable collagen-based bone disorder characterized by low bone mass and pore bone quality and increased fracture risk (Van Dijk and Sillence, 2014). OI is both a genetically and clinically heterogeneous disease that can differ in modes of inheritance and phenotypic presentation ranging in severity from mild forms to perinatally lethal (Marini et al., 2017). Research has largely been focused on the material level property changes directly associated with the altered collagen followed by a focus on the poor mineral quality (Camacho et al., 2003; Surowiec et al., 2020). Water, particularly loosely and tightly bound collagen-related water, is hypothesized to play a role in governing bone health in OI through supporting formation and maintenance of collagen structure and possibly mineralization (Ailavajhala et al., 2020; Kramer et al., 2000). Despite this link, little is known about how bone water is altered under OI conditions. The first mention of bone water in OI came in 2002 where structural modeling suggested that tightly bound water molecules may be increased in OI to help compensate for lost solute hydrogen bond stability observed at the collagen level when OI-causing mutations affecting the *COL1A1* gene are present (Mooney and Klein, 2002).

In pre-clinical testing, NIR spectral analysis in the *oim/oim* (OIM) mouse model of moderate-to-severe OI demonstrated that cortical bone

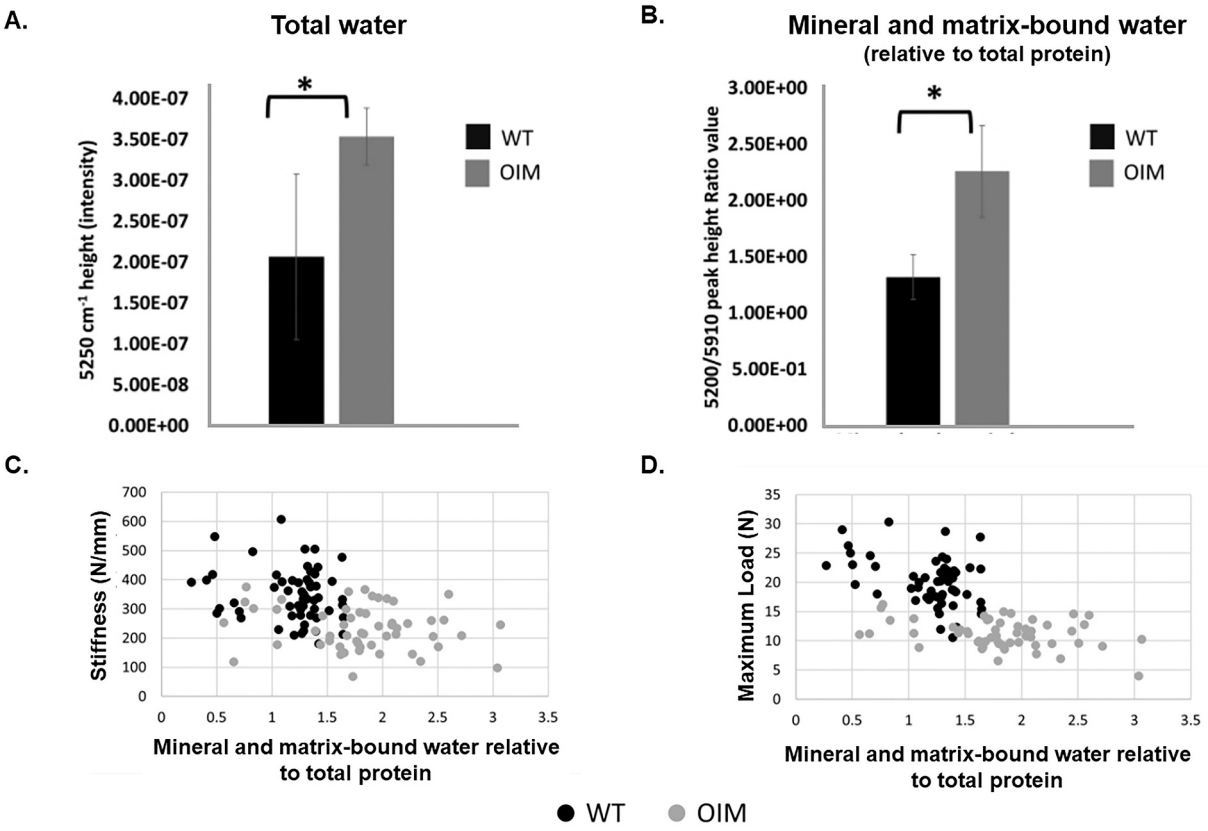

Fig. 10. Higher mineral and matrix-bound water in OIM mice is negatively correlated with stiffness and maximum load. A) Hydrated OIM mouse cortical bone (humerii) had significantly higher total water content compared to wildtype (WT) measured using near-infrared (NIR) spectroscopy (*$p < 0.05$). B) OIM had higher mineral and matrix-bound water content relative to protein in lyophilized samples compared to WT (*$p < 0.05$). C) Mineral and matrix-bound water relative to total protein was negatively correlated to stiffness ($r = -0.44$, $p < 0.05$) and D) maximum load ($r = -0.60$, $p < 0.05$). Figures from Shanas et al. adapted with permission (Shanas et al., 2021).

had a 50% higher overall water content in OIM compared to wildtype controls (Fig. 10A) (Shanas et al., 2021). The authors postulate this was a result of more matrix space in OIM bone for water to 'loosely associate with'. The tightly bound water pool, when considered relative to total matrix content, was higher in OIM mice compared to controls which was negatively correlated with stiffness ($r = -0.44$, $p < 0.05$) and maximum load ($r = -0.60$, $p < 0.05$) suggesting the presence of higher mineralization content (Fig. 10B–D). Similar findings of higher bound water have been reported in the OIM mouse vs. wildtype when atomic force microscopy (AFM) imaging and cantilever-based nanoindentation was carried out in hydrated and dehydrated collagen fibrils (Andriotis et al., 2015). Under air dehydration, the OIM collagen fibrils had lower indentation modulus, greater intermolecular space, and higher remaining water content compared to wildtype collagen fibrils. Because air-dehydration can remove free water, the remaining water represents loosely bound, tightly bound, and structural water. Upon re-hydration in saline, OIM fibrils had a higher indentation modulus (14.2 vs. 2.8 MPa, $p < 0.001$) and decreased fibrillar swelling (42% lower, $p < 0.001$) compared to wildtype. The authors hypothesized the higher remaining bound and structural water content observed during air-dehydration experiments left less room for a further increase to bound water upon rehydration perhaps due to an 'increase of non-enzymatic cross-linking resisting fibril dilation' observed in previous work.

5. Bone hydration as a therapeutic target

Current treatment paradigms for reducing fracture risk are focused on building more bone by increasing osteoblast activity or reduce the rate of bone loss through osteoclast inhibition. While these approaches have been effective, they have limitations (Seeman, 2017). Anti-resorptive agents are the most widely used therapeutic to improve BMD and reduce fracture yet long-term use has been implicated in negative bone quality outcomes. This occurs in part because the suppression of remodeling leads to continual changes in both the mineral and collagen phases, imparting effects that tend to embrittle the matrix, such as increased non-enzymatic collagen crosslinking, microdamage accrual, and increased mineral heterogeneity (Allen et al., 2008; Gourion-Arsiquaud et al., 2010). Each of these effects is known to correlate to poorer mechanical outcomes (Acevedo et al., 2015; Allen and Burr, 2011). Therapeutic modulation of water or the noncollagenous proteins involved in attracting and retaining water, specifically the bound water fraction, represents a novel approach to improve mechanical properties and reduce fracture risk. To date, most of the therapeutic work related to hydration has utilized Raloxifene.

Raloxifene is a selective estrogen receptor modulator (SERM) that functions as an estrogen agonist in the skeleton due to predominant interactions with estrogen receptor alpha (ERα) over ER beta (ERβ) (which would lead to antagonist effects) (Rey et al., 2009). Raloxifene is the generic name for 1-[6-hydroxy-2-(4-hydroxyphenyl)benzo[*b*]thien-3-yl]-1-[4-[2-(1-piperidinyl)ethoxy]phenyl]methanone (Fig. 11A). It has been approved for use since 1997 in the US and 1998 in Europe for the treatment of osteoporosis and as a result of nearly 20 years on the market, has amassed a great deal of data regarding its safety and efficacy. Clinical treatment with RAL has demonstrated significant

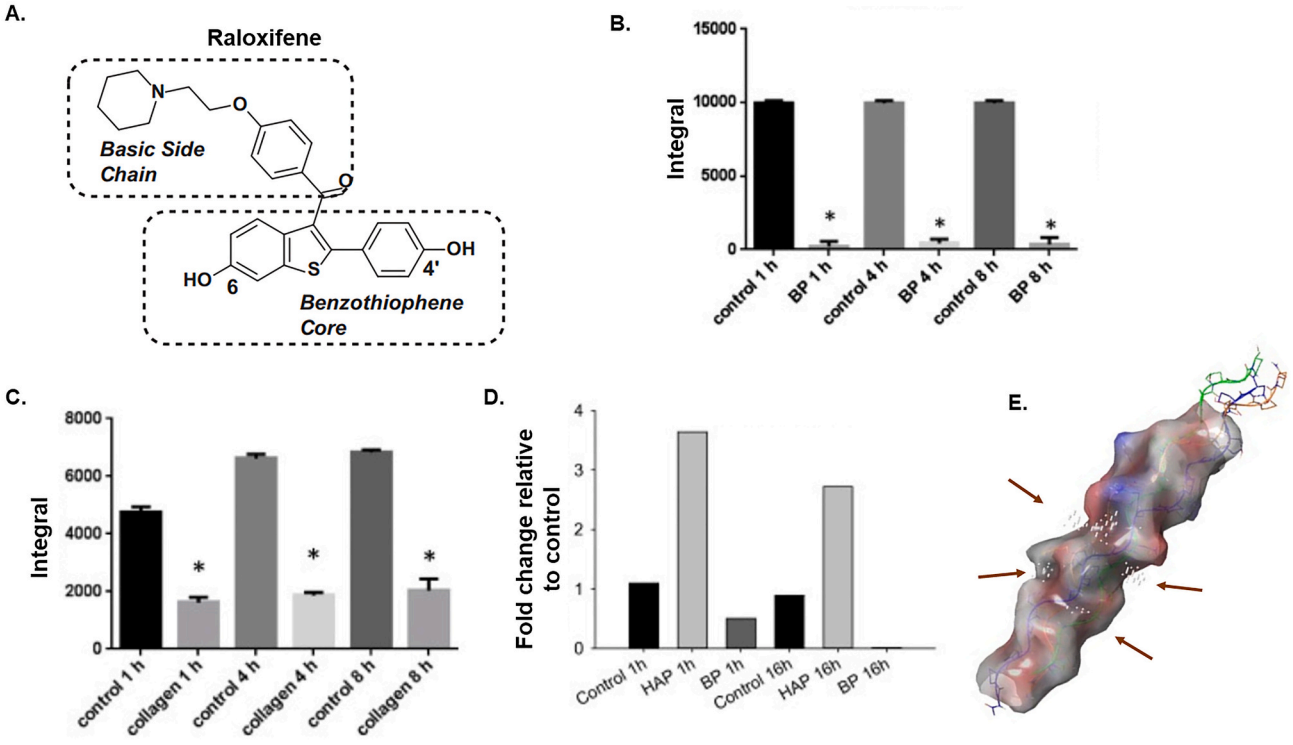

Fig. 11. Raloxifene interacts with collagen, collagen/mineral, but not mineral alone. A) The structural features of RAL include a basic side chain and a benzothiophene core with a hydroxy in 6 and 4′. Detection and relative quantification of RAL in the supernatant after incubation (1, 4, 8 h; 50 μM concentration) without (control) and with 10 mg dog bone powder (B) or collagen (C) using solution state NMR. The amount of RAL in the supernatant was sig. Reduced following incubation with both bone powder and collagen indicating the compound was retained in the bone and by collagen (and no longer in the solution). *$p < 0.05$ by *t*-test vs. control. All graphs represent the integral of the peaks, bars are mean ± standard deviation and each bar is the average of $n = 3$ per group. D) RAL was incubated with bone powder, hydroxyapatite (HAP) or alone (control). HAP incubation did not elicit a decrease but rather resulted in an increase in the amount of RAL recovered in the supernatant while incubation with BP resulted in a 54.2% reduction in signal after 1 h and 99% after 16 h. Bars represent fold change relative to control. $N = 2$. E) The basic side-chain appears to be a crucial structural requirement for bone matrix binding. Molecular modeling using SiteMap shows a collagen triple chain fiber molecular surface with putative binding sites/grooves for RAL indicated by small white spheres near the center (arrows). These grooves have sufficient space to accommodate RAL and are rich with acidic glutamate residues which is consistent with affinity for the basic side chain. Figures from Bivi et al. adapted with permission (Bivi et al., 2016).

decreases in fracture risk (~50%) while only modestly suppressing bone remodeling and minor increases to BMD suggestive of bone quality changes beyond the mineral acting to improve mechanical properties (Ettinger et al., 1999; Riggs and Melton, 2002; Sarkar et al., 2002). Postmenopausal women treated with RAL demonstrated a concurrent increase in total body water, raising the potential that bone water may increase, too (Jacobsen et al., 2010).

Raloxifene has been shown to directly interact with the bone matrix in a cell- and estrogen independent manner (Bivi et al., 2016; Gallant et al., 2014). Non-viable canine bone beams soaked in a solution of raloxifene demonstrated a significantly higher level of matrix bound water (via UTE-MRI) while small angle X-ray scattering during four-point bending showed that raloxifene transferred load between collagen and mineral crystals resulting in lower strain on the mineral and greater overall deformation (Gallant et al., 2014). Further, observations showing increased collagen-D periodic spacing following raloxifene exposure suggest the potential of swelling occurring within the collagen fibrillar structure likely a result of the increased bound water. Using NMR and Fourier transform infrared spectroscopy (FTIR), it was revealed that raloxifene interacts with collagen, collagen/mineral, but not mineral alone and that the interaction is done through its basic sidechain (Fig. 11B–D) (Bivi et al., 2016). When the sidechain is truncated, affinity for binding to the bone is reduced resulting in poorer mechanical outcomes. Using in silico prediction modeling, it has been postulated that groove on the surface of collagen may serve as a likely docking site due to the sufficient space for raloxifene's sidechain (Fig. 11E).

The in vitro effects on hydration have been recapitulated in pre-clinical models. Initial work evaluating raloxifene following one year of treatment in skeletally mature female beagles resulted in significantly more total water in the cortical bone, assessed gravimetrically, compared to controls which positively correlated to mechanical outcomes (Fig. 12A,B) (Gallant et al., 2014). In a separate study, skeletally mature female beagles treated with raloxifene for 6 months of had significantly higher bound water (+14%, $p = 0.05$) and lower free water (−20%, $p = 0.05$) compared to vehicle treated controls measured by UTE-MRI (Fig. 12C) (Allen et al., 2015b). It has been postulated that a pharmaceutical that acts independent of bone cells to exert positive increases in bone material properties would be a prime candidate to use in tandem with other therapies which act by decreasing resorption (bisphosphonates) or enhancing bone building (sclerostin antibody). Thus, when bound water was assessed in beagles treated with raloxifene, alendronate (bisphosphonate), or raloxifene and alendronate, it was observed that the greatest increase in this pool came from raloxifene alone, followed by raloxifene and alendronate, compared to controls (+23% and 18%) and no change from the alendronate group (Fig. 12D) (Allen et al., 2017). This suite of beagle studies using clinically relevant doses of raloxifene has since spurred several important pre-clinical studies looking at the efficacy of raloxifene across animal and disease models and in combination with other bone therapeutics (Eby et al.,

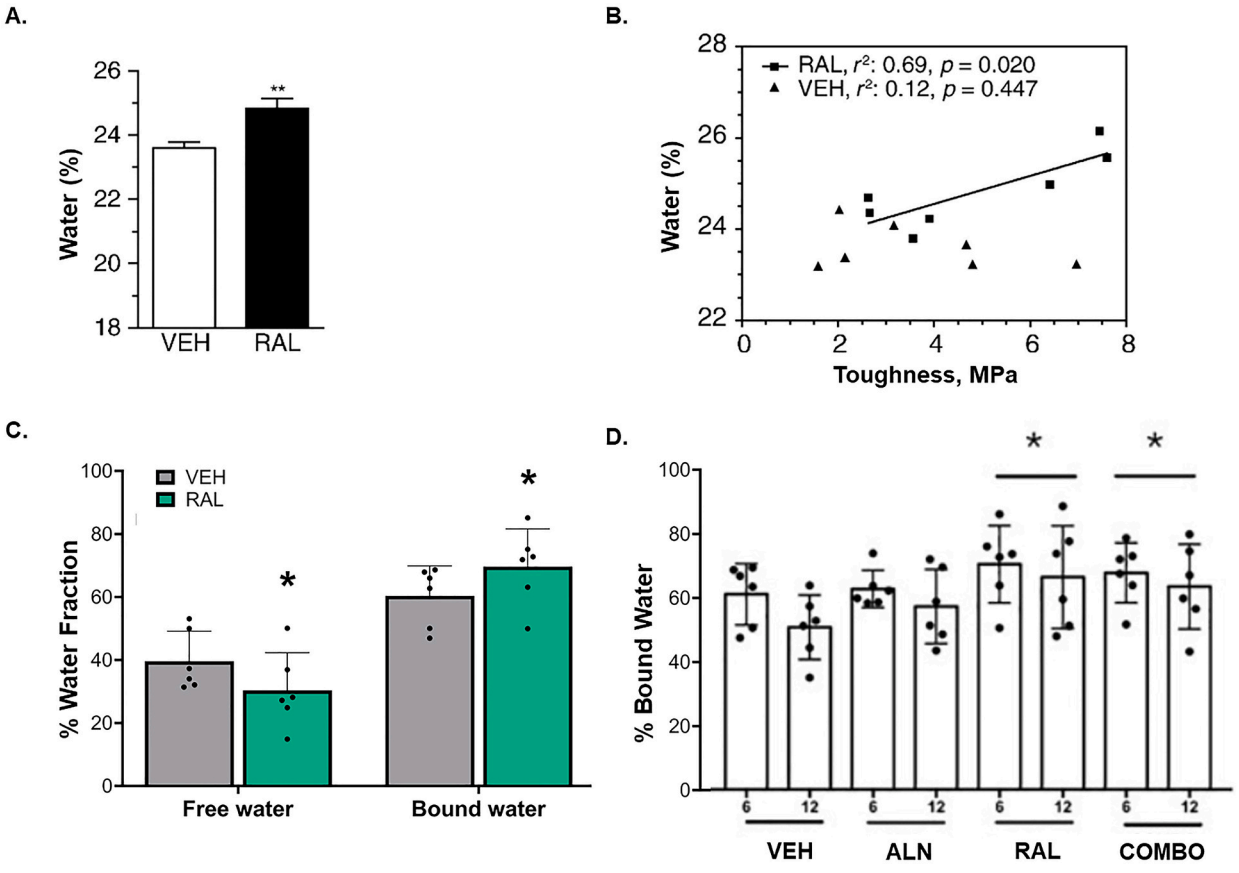

Fig. 12. Raloxifene treatment in vivo increases cortical water. A) Water content measured gravimetrically was significantly higher (+5%) in bone samples from canines treated for 1 year with Raloxifene (RAL, 0.5 mg/kg/day, n = 7) compared to vehicle treated canines (VEH, saline, 1 ml/kg/day, n = 7). **p < 0.01 compared to VEH. B) Water content in canine bone treated for 1 year with RAL positively correlated with bone toughness measured via 4-point bending test. No relationship was observed in VEH treated controls. C) Raloxifene treatment leads to lower free water and higher bound water in cortical bone of skeletally mature female beagles following 6 months of RAL treatment (0.5 mg/kg/day, n = 6) compared to VEH treatment (1 ml/kg/day, n = 6). Water was assessed using UTE-MRI and presented as % water fraction. *p = 0.05 between groups using a one-tailed *t*-test. D) Bound water measured via UTE-MRI at the proximal tibia of skeletally mature female beagles was significantly higher in RAL treated and RAL + alendronate (combo) treated animals relative to VEH. *p < 0.05 when groups were pooled (6 month +12 month, n = 12) relative to VEH groups. Panel A and B (Gallant et al., 2014) and D (Allen et al., 2017) reprinted with permissions. Panel C adapted from Allen et al. (2015b).

2021; Powell et al., 2019; Tastad et al., 2021; Wang et al., 2021a).

Raloxifene's ability to improve bone in an estrogen-independent manner has motivated the synthesis of raloxifene analogs that can reduce and/or eliminate its affinity to ERα. This important modification would thereby mitigate hormone-related side effects making it suitable for a larger portion of the population (e.g., pediatric bone disorders). The first iteration of synthesized analog for bone, raloxifene Analog (RAL-A), replaces 6-hydroxy functionality in raloxifene with a methoxy substitute to create 6′-methoxyraloxifene and demonstrated significantly reduced (but not eliminated) ERα binding while demonstrating the hallmark improved toughness in a preclinical disease model (Powell et al., 2020). Future synthesis work in needed to fully abolish ER binding.

6. Future directions

Imaging advances have greatly enhanced our ability to study water across the bone hierarchy. This has led to a growing understanding of how bone water changes with age and disease and opened the possibility of therapeutically targeting water to improve its mechanical properties. Yet the cycle of research is such that new answers yield exponentially more questions. For example, can water transition between compartments? It has been proposed throughout the literature that tightly bound or structural water molecule is “released” to become a loosely bound or free water molecule in the system (Kerch, 2020). Others have even postulated that collagen-associated water can transition to structural water during mineralization of the osteoid (Nyman et al., 2008) but this would depend upon docking site availability as there is already water associated with the mineral. Further, what regulates the amount of water that can be brought into the matrix? Is there molecular signaling at play or is it more of a passive process that is dictated by physical constituents? And how targetable are each of the compartments to modification and is to what degree can modifications in hydration offset loss of bone mass? These and of course countless other questions which when answered, will no doubt continue to change the way we think and approach enhancing bone health.

CRediT authorship contribution statement

Rachel K. Surowiec: Conceptualization, Writing – original draft. **Matthew R. Allen:** Conceptualization, Writing – review & editing. **Joseph M. Wallace:** Conceptualization, Writing – review & editing.

Declaration of competing interest

Rachel K. Surowiec: No conflict of interest to report.
Matthew R. Allen: No conflict of interest to report.
Joseph M. Wallace: No conflict of interest to report.

Acknowledgements

This work was supported by VA Merit Award (BX003025) from the U.S. Department of Veterans Affairs (Biomedical Laboratory Research and Development Service) to MRA, NSF Award (1952993) to JMW and MRA, NIH Award (R01AR072609) to JMW and the NIH award (T32DK120524) to RKS.

References

Acevedo, C., Bale, H., Gludovatz, B., Wat, A., Tang, S.Y., Wang, M., Busse, B., Zimmermann, E.A., Schaible, E., Allen, M.R., Burr, D.B., Ritchie, R.O., 2015. Alendronate treatment alters bone tissues at multiple structural levels in healthy canine cortical bone. Bone 81, 352–363. https://doi.org/10.1016/j.bone.2015.08.002.

Ailavajhala, R., Oswald, J., Rajapakse, C.S., Pleshko, N., 2019. Environmentally-controlled near infrared spectroscopic imaging of bone water. Scientific Reports 9 (1), 10199. https://doi.org/10.1038/s41598-019-45897-3.

Ailavajhala, R., Querido, W., Rajapakse, C.S., Pleshko, N., 2020. Near infrared spectroscopic assessment of loosely and tightly bound cortical bone water. Analyst 145 (10), 3713–3724. https://doi.org/10.1039/c9an02491c.

Akbari, A., Abbasi-Rad, S., Rad, H.S., 2016. T1 correlates age: a short-TE MR relaxometry study in vivo on human cortical bone free water at 1.5T. Bone 83, 17–22. https://doi.org/10.1016/j.bone.2015.10.006.

Alexander, B., Daulton, T.L., Genin, G.M., Lipner, J., Pasteris, J.D., Wopenka, B., Thomopoulos, S., 2012. The nanometre-scale physiology of bone: steric modelling and scanning transmission electron microscopy of collagen-mineral structure. J. R. Soc. Interface 9 (73), 1774–1786. https://doi.org/10.1098/rsif.2011.0880.

Allen, M.R., Burr, D.B., 2011. Bisphosphonate effects on bone turnover, microdamage, and mechanical properties: what we think we know and what we know that we don't know. Bone 49 (1), 56–65. https://doi.org/10.1016/j.bone.2010.10.159.

Allen, M.R., Gineyts, E., Leeming, D.J., Burr, D.B., Delmas, P.D., 2008. Bisphosphonates alter trabecular bone collagen cross-linking and isomerization in beagle dog vertebra. Osteoporos. Int. 19 (3), 329–337. https://doi.org/10.1007/s00198-007-0533-7.

Allen, M.R., Newman, C.L., Chen, N., Granke, M., Nyman, J.S., Moe, S.M., 2015. Changes in skeletal collagen cross-links and matrix hydration in high- and low-turnover chronic kidney disease. Osteoporos. Int. 26 (3), 977–985. https://doi.org/10.1007/s00198-014-2978-9.

Allen, M.R., Territo, P.R., Lin, C., Persohn, S., Jiang, L., Riley, A.A., McCarthy, B.P., Newman, C.L., Burr, D.B., Hutchins, G.D., 2015. In vivo UTE-MRI reveals positive effects of raloxifene on skeletal-bound water in skeletally mature beagle dogs. J. Bone Miner. Res. 30 (8), 1441–1444. https://doi.org/10.1002/jbmr.2470.

Allen, M.R., McNerny, E., Aref, M., Organ, J.M., Newman, C.L., McGowan, B., Jang, T., Burr, D.B., Brown, D.M., Hammond, M., Territo, P.R., Lin, C., Persohn, S., Jiang, L., Riley, A.A., McCarthy, B.P., Hutchins, G.D., Wallace, J.M., 2017. Effects of combination treatment with alendronate and raloxifene on skeletal properties in a beagle dog model. PLoS One 12 (8), e0181750. https://doi.org/10.1371/journal.pone.0181750.

Andriotis, O.G., Chang, S.W., Vanleene, M., Howarth, P.H., Davies, D.E., Shefelbine, S.J., Buehler, M.J., Thurner, P.J., 2015. Structure–mechanics relationships of collagen fibrils in the osteogenesis imperfecta mouse model. J. R. Soc. Interface 12 (111), 20150701. https://doi.org/10.1098/rsif.2015.0701.

Bae, W.C., Chen, P.C., Chung, C.B., Masuda, K., D'Lima, D., Du, J., 2012. Quantitative ultrashort echo time (UTE) MRI of human cortical bone: correlation with porosity and biomechanical properties. J. Bone Miner. Res. 27 (4), 848–857. https://doi.org/10.1002/jbmr.1535.

Bae, W.C., Chen, P.C., Chung, C.B., Masuda, K., D'Lima, D., Du, J., 2012. Quantitative ultrashort echo time (UTE) MRI of human cortical bone: correlation with porosity and biomechanical properties. J. Bone Miner. Res. 27 (4), 848–857. https://doi.org/10.1002/jbmr.1535.

Beard, P., 2011. Biomedical photoacoustic imaging. Interface Focus 1 (4), 602–631. https://doi.org/10.1098/rsfs.2011.0028.

Bella, J., Brodsky, B., Berman, H.M., 1995. Hydration structure of a collagen peptide. Structure 3 (9), 893–906. https://doi.org/10.1016/s0969-2126(01)00224-6.

Bergholt, M., Serio, A., Albro, M., 2019. Raman spectroscopy: guiding light for the extracellular matrix. Front. Bioeng. Biotechnol. 7 (303) https://doi.org/10.3389/fbioe.2019.00303.

Best, S.M., Duer, M.J., Reid, D.G., Wise, E.R., Zou, S., 2008. Towards a model of the mineral-organic interface in bone: NMR of the structure of synthetic glycosaminoglycan- and polyaspartate-calcium phosphate composites. Magn. Reson. Chem. 46 (4), 323–329. https://doi.org/10.1002/mrc.2168.

Biswas, R., Bae, W., Diaz, E., Masuda, K., Chung, C.B., Bydder, G.M., Du, J., 2012. Ultrashort echo time (UTE) imaging with bi-component analysis: bound and free water evaluation of bovine cortical bone subject to sequential drying. Bone 50 (3), 749–755. https://doi.org/10.1016/j.bone.2011.11.029.

Bivi, N., Hu, H., Chavali, B., Chalmers, M.J., Reutter, C.T., Durst, G.L., Riley, A., Sato, M., Allen, M.R., Burr, D.B., Dodge, J.A., 2016. Structural features underlying raloxifene's biophysical interaction with bone matrix. Bioorg. Med. Chem. 24 (4), 759–767. https://doi.org/10.1016/j.bmc.2015.12.045.

Boskey, A.L., Robey, P.G., 2018. The composition of bone, primer on the metabolic bone diseases and disorders of mineral. Metabolism 84–92.

Boughton, O.R., Ma, S., Cai, X., Yan, L., Peralta, L., Laugier, P., Marrow, J., Giuliani, F., Hansen, U., Abel, R.L., Grimal, Q., Cobb, J.P., 2019. Computed tomography porosity and spherical indentation for determining cortical bone millimetre-scale mechanical properties. Sci Rep 9 (1), 7416. https://doi.org/10.1038/s41598-019-43686-6 passim.

Bridelli, M.G., Chiaramaria, S., Bedotti, R., 2017. Fourier transform infrared conformational investigation of type I collagen aged by in vitro induced dehydration and non-enzymatic glycation treatments. J. Biol. Res. 90 (1) https://doi.org/10.4081/jbr.2017.6254.

Brodsky, B., Persikov, A.V., 2005. In: Molecular Structure of the Collagen Triple Helix, Advances in Protein Chemistry. Academic Press, pp. 301–339.

Brown, S.P., 2012. Applications of high-resolution 1H solid-state NMR. Solid State Nucl. Magn. Reson. 41, 1–27. https://doi.org/10.1016/j.ssnmr.2011.11.006.

Burr, D.B., Turner, C.H., 1999. CHAPTER 26 - biomechanical measurements in age-related bone loss. In: Rosen, C.J., Glowacki, J., Bilezikian, J.P. (Eds.), The Aging Skeleton. Academic Press, San Diego, pp. 301–311.

Camacho, N.P., Carroll, P., Raggio, C.L., 2003. Fourier transform infrared imaging spectroscopy (FT-IRIS) of mineralization in bisphosphonate-treated oim/oim mice. Calcif. Tissue Int. 72 (5), 604–609. https://doi.org/10.1007/s00223-002-1038-1.

Cao, H., Ackerman, J.L., Hrovat, M.I., Graham, L., Glimcher, M.J., Wu, Y., 2008. Quantitative bone matrix density measurement by water- and fat-suppressed proton

projection MRI (WASPI) with polymer calibration phantoms. Magn. Reson. Med. 60 (6), 1433–1443. https://doi.org/10.1002/mrm.21771.
Casciani, F., 1971. Identification of hydrate water in enamel, dentine, cementum and bone. In: Fearnhead, R.S., MV (Eds.), Tooth Enamel II: its composition, properties and fundamental structure. John Wright & Sons, Ltd, Bristol, pp. 14–23.
Chang, E.Y., Bae, W.C., Shao, H., Biswas, R., Li, S., Chen, J., Patil, S., Healey, R., D'Lima, D.D., Chung, C.B., Du, J., 2015. Ultrashort echo time magnetization transfer (UTE-MT) imaging of cortical bone. NMR Biomed. 28 (7), 873–880. https://doi.org/10.1002/nbm.3316.
Chang, E.Y., Du, J., Chung, C.B., 2015. UTE imaging in the musculoskeletal system. J. Magn. Reson. Imaging 41 (4), 870–883. https://doi.org/10.1002/jmri.24713.
Chang, G., Boone, S., Martel, D., Rajapakse, C.S., Hallyburton, R., Valko, M., Honig, S., Regatte, R.R., 2017. MRI assessment of bone structure and microarchitecture. J. Magn. Reson. Imaging 46 (2), 323–337. https://doi.org/10.1002/jmri.25647.
Chen, M., Yuan, H., 2018. Assessment of porosity index of the femoral neck and tibia by 3D ultra-short echo-time MRI. J. Magn. Reson. Imaging 47 (3), 820–828. https://doi.org/10.1002/jmri.25782.
Choksi, P., Jepsen, K.J., Clines, G.A., 2018. The challenges of diagnosing osteoporosis and the limitations of currently available tools. Clin. Diabetes Endocrinol. 4, 12. https://doi.org/10.1186/s40842-018-0062-7.
Creecy, A., Uppuganti, S., Girard, M.R., Schlunk, S.G., Amah, C., Granke, M., Unal, M., Does, M.D., Nyman, J.S., 2020. The age-related decrease in material properties of BALB/c mouse long bones involves alterations to the extracellular matrix. Bone 130, 115126. https://doi.org/10.1016/j.bone.2019.115126.
Damilakis, J., Adams, J.E., Guglielmi, G., Link, T.M., 2010. Radiation exposure in X-ray-based imaging techniques used in osteoporosis. Eur. Radiol. 20 (11), 2707–2714. https://doi.org/10.1007/s00330-010-1845-0.
Davies, E., Muller, K.H., Wong, W.C., Pickard, C.J., Reid, D.G., Skepper, J.N., Duer, M.J., 2014. Citrate bridges between mineral platelets in bone. Proc. Natl. Acad. Sci. U. S. A. 111 (14), E1354–E1363. https://doi.org/10.1073/pnas.1315080111.
Dempster, W.T., Liddicoat, R.T., 1952. Compact bone as a non-isotropic material. Am. J. Anat. 91 (3), 331–362. https://doi.org/10.1002/aja.1000910302.
Donnelly, E., Boskey, A.L., Baker, S.P., van der Meulen, M.C.H., 2010. Effects of tissue age on bone tissue material composition and nanomechanical properties in the rat cortex. J. Biomed. Mater. Res. A 92 (3), 1048–1056. https://doi.org/10.1002/jbm.a.32442.
Drouet, C., Aufray, M., Rollin-Martinet, S., Vandecandelaere, N., Grossin, D., Rossignol, F., 2018. Nanocrystalline apatites: the fundamental role of water. Am. Mineral. 103 (4), 550–564. https://doi.org/10.2138/am-2018-6415.
Du, J., Carl, M., Bydder, M., Takahashi, A., Chung, C.B., Bydder, G.M., 2010. Qualitative and quantitative ultrashort echo time (UTE) imaging of cortical bone. J. Magn. Reson. 207 (2), 304–311. https://doi.org/10.1016/j.jmr.2010.09.013.
Duer, M., Veis, A., 2013. Bone mineralization: water brings order. Nat. Mater. 12 (12), 1081–1082. https://doi.org/10.1038/nmat3822.
Eberhardsteiner, L., Hellmich, C., Scheiner, S., 2014. Layered water in crystal interfaces as source for bone viscoelasticity: arguments from a multiscale approach. Comput Methods Biomech Biomed Engin 17 (1), 48–63. https://doi.org/10.1080/10255842.2012.670227.
Eby, M.R., Cristino, D.M., Counihan, M., Masada, K.M., Ahn, J., Hast, M.W., 2021. Immersion in Raloxifene does not significantly improve bone toughness or screw pull-out strength in multiple in vitro models. BMC Musculoskelet Disord 22 (1), 468. https://doi.org/10.1186/s12891-021-04342-1.
Elliott, S.R., Robinson, R.A., 1957. The water content of bone. I. The mass of water, inorganic crystals, organic matrix, and CO2 space components in a unit volume of the dog bone. J. Bone Joint Surg. Am. 39-A (1), 167–188.
Ettinger, B., Black, D.M., Mitlak, B.H., Knickerbocker, R.K., Nickelsen, T., Genant, H.K., Christiansen, C., Delmas, P.D., Zanchetta, J.R., Stakkestad, J., Glüer, C.C., Krueger, K., Cohen, F.J., Eckert, S., Ensrud, K.E., Avioli, L.V., Lips, P., Cummings, S. R., 1999. Reduction of vertebral fracture risk in postmenopausal women with osteoporosis treated with raloxifene: results from a 3-year randomized clinical trial. Multiple Outcomes of Raloxifene Evaluation (MORE) Investigators. Jama 282 (7), 637–645. https://doi.org/10.1001/jama.282.7.637.
Evans, F.G., 1973. Factors affecting the mechanical properties of bone. Bull. N. Y. Acad. Med. 49 (9), 751–764.
Evans, F.G., Lebow, M., 1951. Regional differences in some of the physical properties of the human femur. J. Appl. Physiol. 3 (9), 563–572. https://doi.org/10.1152/jappl.1951.3.9.563.
Faingold, A., Cohen, S.R., Shahar, R., Weiner, S., Rapoport, L., Wagner, H.D., 2014. The effect of hydration on mechanical anisotropy, topography and fibril organization of the osteonal lamellae. J. Biomech. 47 (2), 367–372. https://doi.org/10.1016/j.jbiomech.2013.11.022.
Fantazzini, P., Brown, R.J., Borgia, G.C., 2003. Bone tissue and porous media: common features and differences studied by NMR relaxation. Magn. Reson. Imaging 21 (3–4), 227–234. https://doi.org/10.1016/s0730-725x(03)00129-2.
Fantazzini, P., Bortolotti, V., Brown, R.J., Camaiti, M., Garavaglia, C., Viola, R., Giavaresi, G., 2004. Two 1H-nuclear magnetic resonance methods to measure internal porosity of bone trabeculae: by solid–liquid signal separation and by longitudinal relaxation. J. Appl. Phys. 95 (1), 339–343. https://doi.org/10.1063/1.1630374.
Farr, J.N., Khosla, S., 2016. Determinants of bone strength and quality in diabetes mellitus in humans. Bone 82, 28–34. https://doi.org/10.1016/j.bone.2015.07.027.
Feng, T., Perosky, J.E., Kozloff, K.M., Xu, G., Cheng, Q., Du, S., Yuan, J., Deng, C.X., Wang, X., 2015. Characterization of bone microstructure using photoacoustic spectrum analysis. Opt. Express 23 (19), 25217–25224. https://doi.org/10.1364/OE.23.025217.
Feng, T., Zhu, Y., Morris, R., Kozloff, K.M., Wang, X., 2020. Functional Photoacoustic and Ultrasonic Assessment of Osteoporosis: A Clinical Feasibility Study. BMEF. https://doi.org/10.34133/2020/1081540, 1081540.
Feng, T., Ge, Y., Xie, Y., Xie, W., Liu, C., Li, L., Ta, D., Jiang, Q., Cheng, Q., 2021. Detection of collagen by multi-wavelength photoacoustic analysis as a biomarker for bone health assessment. Photoacoustics 24, 100296. https://doi.org/10.1016/j.pacs.2021.100296.
Ferguson, V.L., 2009. Deformation partitioning provides insight into elastic, plastic, and viscous contributions to bone material behavior. J. Mech. Behav. Biomed. Mater. 2 (4), 364–374. https://doi.org/10.1016/j.jmbbm.2009.01.004.
Fernandez-Seara, M.A., Wehrli, S.L., Takahashi, M., Wehrli, F.W., 2004. Water content measured by proton-deuteron exchange NMR predicts bone mineral density and mechanical properties. J. Bone Miner. Res. 19 (2), 289–296. https://doi.org/10.1359/JBMR.0301227.
Gallant, M.A., Brown, D.M., Hammond, M., Wallace, J.M., Du, J., Deymier-Black, A.C., Almer, J.D., Stock, S.R., Allen, M.R., Burr, D.B., 2014. Bone cell-independent benefits of raloxifene on the skeleton: a novel mechanism for improving bone material properties. Bone 61, 191–200. https://doi.org/10.1016/j.bone.2014.01.009.
Garner, E., Lakes, R., Lee, T., Swan, C., Brand, R., 2000. Viscoelastic dissipation in compact bone: implications for stress-induced fluid flow in bone. J. Biomech. Eng. 122 (2), 166–172. https://doi.org/10.1115/1.429638.
Gourion-Arsiquaud, S., Allen, M.R., Burr, D.B., Vashishth, D., Tang, S.Y., Boskey, A.L., 2010. Bisphosphonate treatment modifies canine bone mineral and matrix properties and their heterogeneity. Bone 46 (3), 666–672. https://doi.org/10.1016/j.bone.2009.11.011.
Granke, M., Does, M.D., Nyman, J.S., 2015. The role of water compartments in the material properties of cortical bone. Calcif. Tissue Int. 97 (3), 292–307. https://doi.org/10.1007/s00223-015-9977-5.
Granke, M., Makowski, A.J., Uppuganti, S., Does, M.D., Nyman, J.S., 2015. Identifying novel clinical surrogates to assess human bone fracture toughness. J. Bone Miner. Res. 30 (7), 1290–1300. https://doi.org/10.1002/jbmr.2452.
Hafner, S., 1994. Fast imaging in liquids and solids with the Back-projection low angle ShoT (BLAST) technique. Magn. Reson. Imaging 12 (7), 1047–1051. https://doi.org/10.1016/0730-725x(94)91236-p.
Han, Y., Gomez, J., Hua, R., Xiao, P., Gao, W., Jiang, J.X., Wang, X., 2021. Removal of glycosaminoglycans affects the in situ mechanical behavior of extrafibrillar matrix in bone. J. Mech. Behav. Biomed. Mater. 123, 104766 https://doi.org/10.1016/j.jmbbm.2021.104766.
Hashimoto, Y., Lester, G.E., Caterson, B., Yamauchi, M., 1995. EDTA-insoluble, calcium-binding proteoglycan in bovine bone. Calcif. Tissue Int. 56 (5), 398–402. https://doi.org/10.1007/BF00301609.
Henrotin, Y., Mathy, M., Sanchez, C., Lambert, C., 2010. Chondroitin sulfate in the treatment of osteoarthritis: from in vitro studies to clinical recommendations. Ther. Adv. Musculoskelet. Dis. 2 (6), 335–348. https://doi.org/10.1177/1759720X10383076.
Hernandez, C.J., van der Meulen, M.C., 2017. Understanding bone strength is not enough. J. Bone Miner. Res. 32 (6), 1157–1162. https://doi.org/10.1002/jbmr.3078.
Hodgkinson, P., Wimperis, S., 2009. Solid-state NMR spectroscopy. Phys Chem Chem Phys 11 (32), 6875. https://doi.org/10.1039/b914008p.
Hong, A.L., Ispiryan, M., Padalkar, M.V., Jones, B.C., Batzdorf, A.S., Shetye, S.S., Pleshko, N., Rajapakse, C.S., 2019. MRI-derived bone porosity index correlates to bone composition and mechanical stiffness. Bone Rep. 11, 100213 https://doi.org/10.1016/j.bonr.2019.100213.
Horch, R., Nyman, J.S., Gochberg, D.F., Dortch, R.D., Does, M.D., 2010. Characterization of 1H NMR signal in human cortical bone for magnetic resonance imaging. Magn. Reson. Med. 64 (3), 680–687. https://doi.org/10.1002/mrm.22459.
Horch, R., Gochberg, D., Nyman, J., Does, M., 2011. Non-invasive predictors of human cortical bone mechanical properties: T(2)-discriminated H NMR compared with high resolution X-ray. PLoS One 6 (1), e16359. https://doi.org/10.1371/journal.pone.0016359.
Horch, R., Gochberg, D.F., Nyman, J.S., Does, M.D., 2012. Clinically compatible MRI strategies for discriminating bound and pore water in cortical bone. Magn. Reson. Med. 68 (6), 1774–1784. https://doi.org/10.1002/mrm.24186.
Hua, R., Ni, Q., Eliason, T.D., Han, Y., Gu, S., Nicolella, D.P., Wang, X., Jiang, J.X., 2020. Biglycan and chondroitin sulfate play pivotal roles in bone toughness via retaining bound water in bone mineral matrix. Matrix Biol. 94, 95–109. https://doi.org/10.1016/j.matbio.2020.09.002.
Hui, S.L., Slemenda, C.W., Johnston Jr., C.C., 1988. Age and bone mass as predictors of fracture in a prospective study. J. Clin. Invest. 81 (6), 1804–1809. https://doi.org/10.1172/jci113523.
Idiyatullin, D., Corum, C., Park, J.Y., Garwood, M., 2006. Fast and quiet MRI using a swept radiofrequency. J. Magn. Reson. 181 (2), 342–349. https://doi.org/10.1016/j.jmr.2006.05.014.
Ivanchenko, P., Delgado-Lopez, J.M., Iafisco, M., Gomez-Morales, J., Tampieri, A., Martra, G., Sakhno, Y., 2017. On the surface effects of citrates on nano-apatites: evidence of a decreased hydrophilicity. Sci Rep 7 (1), 8901. https://doi.org/10.1038/s41598-017-09376-x.
Iwasaki, Y., Kazama, J.J., Yamato, H., Matsugaki, A., Nakano, T., Fukagawa, M., 2015. Altered material properties are responsible for bone fragility in rats with chronic kidney injury. Bone 81, 247–254. https://doi.org/10.1016/j.bone.2015.07.015.
Jacobsen, D.E., Samson, M.M., Emmelot-Vonk, M.H., Verhaar, H.J., 2010. Raloxifene and body composition and muscle strength in postmenopausal women: a randomized, double-blind, placebo-controlled trial. Eur. J. Endocrinol. 162 (2), 371–376. https://doi.org/10.1530/eje-09-0619.

Jazini, E., Sharan, A.D., Morse, L.J., Dyke, J.P., Aronowitz, E.B., Chen, L.K., Tang, S.Y., 2012. Alterations in T2 relaxation magnetic resonance imaging of the ovine intervertebral disc due to nonenzymatic glycation. Spine (Phila Pa 1976) 37 (4), E209-15. https://doi.org/10.1097/BRS.0b013e31822ce81f.

Jerban, S., Ma, Y., Nazaran, A., Dorthe, E.W., Cory, E., Carl, M., D'Lima, D., Sah, R.L., Chang, E.Y., Du, J., 2018. Detecting stress injury (fatigue fracture) in fibular cortical bone using quantitative ultrashort echo time-magnetization transfer (UTE-MT): an ex vivo study. NMR Biomed 31 (11), e3994. https://doi.org/10.1002/nbm.3994.

Jerban, S., Ma, Y., Li, L., Jang, H., Wan, L., Guo, T., Searleman, A., Chang, E.Y., Du, J., 2019. Volumetric mapping of bound and pore water as well as collagen protons in cortical bone using 3D ultrashort echo time cones MR imaging techniques. Bone 127, 120–128. https://doi.org/10.1016/j.bone.2019.05.038.

Jerban, S., Ma, Y., Wong, J.H., Nazaran, A., Searleman, A., Wan, L., Williams, J., Du, J., Chang, E.Y., 2019. Ultrashort echo time magnetic resonance imaging (UTE-MRI) of cortical bone correlates well with histomorphometric assessment of bone microstructure. Bone 123, 8–17. https://doi.org/10.1016/j.bone.2019.03.013.

Jerban, S., Lu, X., Dorthe, E.W., Alenezi, S., Ma, Y., Kakos, L., Jang, H., Sah, R.L., Chang, E.Y., D'Lima, D., Du, J., 2020. Correlations of cortical bone microstructural and mechanical properties with water proton fractions obtained from ultrashort echo time (UTE) MRI tricomponent T2* model. NMR Biomed. 33 (3), e4233. https://doi.org/10.1002/nbm.4233.

Jerban, S., Ma, Y., Jang, H., Namiranian, B., Le, N., Shirazian, H., Murphy, M.E., Du, J., Chang, E.Y., 2020. Water proton density in human cortical bone obtained from ultrashort echo time (UTE) MRI predicts bone microstructural properties. Magn. Reson. Imaging 67, 85–89. https://doi.org/10.1016/j.mri.2020.01.004.

Jerban, S., Ma, Y., Wei, Z., Jang, H., Chang, E.Y., Du, J., 2020. Quantitative magnetic resonance imaging of cortical and trabecular bone. Semin. Musculoskelet. Radiol. 24 (04), 386–401.

Jones, R.R., Hooper, D.C., Zhang, L., Wolverson, D., Valev, V.K., 2019. Raman techniques: fundamentals and frontiers. Nanoscale Res. Lett. 14 (1), 231. https://doi.org/10.1186/s11671-019-3039-2.

Jones, B.C., Jia, S., Lee, H., Feng, A., Shetye, S.S., Batzdorf, A., Shapira, N., Noel, P.B., Pleshko, N., Rajapakse, C.S., 2021. MRI-derived porosity index is associated with whole-bone stiffness and mineral density in human cadaveric femora. Bone 143, 115774. https://doi.org/10.1016/j.bone.2020.115774.

Kahler, B., Swain, M.V., Moule, A., 2003. Fracture-toughening mechanisms responsible for differences in work to fracture of hydrated and dehydrated dentine. J. Biomech. 36 (2), 229–237. https://doi.org/10.1016/s0021-9290(02)00327-5.

Kanis, J.A., 1994. Assessment of fracture risk and its application to screening for postmenopausal osteoporosis: synopsis of a WHO report. WHO Study Group. Osteoporos. Int. 4 (6), 368–381. https://doi.org/10.1007/bf01622200.

Kanis, J.A., 2002. Diagnosis of osteoporosis and assessment of fracture risk. Lancet 359 (9321), 1929–1936. https://doi.org/10.1016/S0140-6736(02)08761-5.

Kanis, J.A., Johnell, O., Oden, A., Dawson, A., De Laet, C., Jonsson, B., 2001. Ten year probabilities of osteoporotic fractures according to BMD and diagnostic thresholds. Osteoporos. Int. 12 (12), 989–995. https://doi.org/10.1007/s001980170006.

Katsamenis, O.L., Jenkins, T., Thurner, P.J., 2015. Toughness and damage susceptibility in human cortical bone is proportional to mechanical inhomogeneity at the osteonal-level. Bone 76, 158–168. https://doi.org/10.1016/j.bone.2015.03.020.

Kerch, G., 2020. Role of changes in state of bound water and tissue stiffness in development of age-related diseases. Polymers (Basel) 12 (6). https://doi.org/10.3390/polym12061362.

Koester, K.J., Barth, H.D., Ritchie, R.O., 2011. Effect of aging on the transverse toughness of human cortical bone: evaluation by R-curves. J. Mech. Behav. Biomed. Mater. 4 (7), 1504–1513. https://doi.org/10.1016/j.jmbbm.2011.05.020.

Kopp, J., Bonnet, M., Renou, J.P., 1989. Effect of collagen crosslinking on collagen-water interactions (a DSC investigation). Matrix 9 (6), 443–450. https://doi.org/10.1016/s0934-8832(11)80013-2.

Kramer, R.Z., Venugopal, M.G., Bella, J., Mayville, P., Brodsky, B., Berman, H.M., 2000. Staggered molecular packing in crystals of a collagen-like peptide with a single charged pair. J. Mol. Biol. 301 (5), 1191–1205. https://doi.org/10.1006/jmbi.2000.4017.

Laperre, K., Depypere, M., van Gastel, N., Torrekens, S., Moermans, K., Bogaerts, R., Maes, F., Carmeliet, G., 2011. Development of micro-CT protocols for in vivo follow-up of mouse bone architecture without major radiation side effects. Bone 49 (4), 613–622. https://doi.org/10.1016/j.bone.2011.06.031.

Lashkari, B., Mandelis, A., 2014. Coregistered photoacoustic and ultrasonic signatures of early bone density variations. J. Biomed. Opt. 19 (3), 036015.

Lazarev, Y.A., Grishkovsky, B.A., Khromova, T.B., Lazareva, A.V., Grechishko, V.S., 1992. Bound water in the collagen-like triple-helical structure. Biopolymers 32 (2), 189–195. https://doi.org/10.1002/bip.360320209.

Lees, S., 1981. A mixed packing model for bone collagen. Calcif. Tissue Int. 33 (6), 591–602. https://doi.org/10.1007/BF02409497.

Li, S., Ma, L., Chang, E.Y., Shao, H., Chen, J., Chung, C.B., Bydder, G.M., Du, J., 2015. Effects of inversion time on inversion recovery prepared ultrashort echo time (IR-UTE) imaging of bound and pore water in cortical bone. NMR Biomed. 28 (1), 70–78. https://doi.org/10.1002/nbm.3228.

Lin, E.C., 2010. Radiation risk from medical imaging. Mayo Clin Proc 85 (12), 1142–1146. https://doi.org/10.4065/mcp.2010.0260 quiz 1146.

Liu, J., Hou, Z., Qin, Q.-H., Fu, D., Pan, S., 2019. Variation of streaming potentials with time under steady fluid pressure in bone. Appl. Sci. 9 (18), 3726.

Lorentzon, M., Cummings, S.R., 2015. Osteoporosis: the evolution of a diagnosis. J. Intern. Med. 277 (6), 650–661. https://doi.org/10.1111/joim.12369.

Lu, X., Jerban, S., Wan, L., Ma, Y., Jang, H., Le, N., Yang, W., Chang, E.Y., Du, J., 2019. Three-dimensional ultrashort echo time imaging with tricomponent analysis for human cortical bone. Magn. Reson. Med. 82 (1), 348–355. https://doi.org/10.1002/mrm.27718.

Ma, Y., Shao, H., Du, J., Chang, E.Y., 2016. Ultrashort echo time magnetization transfer (UTE-MT) imaging and modeling: magic angle independent biomarkers of tissue properties. NMR Biomed. 29 (11), 1546–1552. https://doi.org/10.1002/nbm.3609.

Ma, Y., Chang, E.Y., Carl, M., Du, J., 2018. Quantitative magnetization transfer ultrashort echo time imaging using a time-efficient 3D multispoke cones sequence. Magn. Reson. Med. 79 (2), 692–700. https://doi.org/10.1002/mrm.26716.

Ma, Y.J., Jerban, S., Jang, H., Chang, D., Chang, E.Y., Du, J., 2020. Quantitative ultrashort Echo time (UTE) magnetic resonance imaging of bone: an update. Front. Endocrinol. (Lausanne) 11, 567417. https://doi.org/10.3389/fendo.2020.567417.

Ma, Y.J., Jerban, S., Jang, H., Chang, D., Chang, E.Y., Du, J., 2020. Quantitative ultrashort Echo time (UTE) magnetic resonance imaging of bone: an update. Front. Endocrinol. (Lausanne) 11, 567417. https://doi.org/10.3389/fendo.2020.567417.

Madio, D.P., Lowe, I.J., 1995. Ultra-fast imaging using low flip angles and FIDs. Magn. Reson. Med. 34 (4), 525–529. https://doi.org/10.1002/mrm.1910340407.

Maghsoudi-Ganjeh, M., Wang, X., Zeng, X., 2020. Computational investigation of the effect of water on the nanomechanical behavior of bone. J. Mech. Behav. Biomed. Mater. 101, 103454 https://doi.org/10.1016/j.jmbbm.2019.103454.

Mahesh, M., 2013. The essential physics of medical imaging, third edition. Med. Phys. 40 (7) https://doi.org/10.1118/1.4811156.

Makowski, A.J., Granke, M., Ayala, O.D., Uppuganti, S., Mahadevan-Jansen, A., Nyman, J.S., 2017. Applying full Spectrum analysis to a raman spectroscopic assessment of fracture toughness of human cortical bone. Appl. Spectrosc. 71 (10), 2385–2394. https://doi.org/10.1177/0003702817718149.

Manhard, M.K., Horch, R.A., Gochberg, D.F., Nyman, J.S., Does, M.D., 2015. In vivo quantitative MR imaging of bound and pore water in cortical bone. Radiology 277 (1), 221–229. https://doi.org/10.1148/radiol.2015140336.

Manhard, M.K., Uppuganti, S., Granke, M., Gochberg, D.F., Nyman, J.S., Does, M.D., 2016. MRI-derived bound and pore water concentrations as predictors of fracture resistance. Bone 87, 1–10. https://doi.org/10.1016/j.bone.2016.03.007.

Marcon, M., Keller, D., Wurnig, M.C., Weiger, M., Kenkel, D., Eberhardt, C., Eberli, D., Boss, A., 2017. Separation of collagen-bound and porous bone-water longitudinal relaxation in mice using a segmented inversion recovery zero-echo-time sequence. Magn. Reson. Med. 77 (5), 1909–1915. https://doi.org/10.1002/mrm.26277.

Marini, J.C., Forlino, A., Bächinger, H.P., Bishop, N.J., Byers, P.H., Paepe, A., Fassier, F., Fratzl-Zelman, N., Kozloff, K.M., Krakow, D., Montpetit, K., Semler, O., 2017. Osteogenesis imperfecta. Nat. Rev. Dis. Primers 3, 17052. https://doi.org/10.1038/nrdp.2017.52.

Marino, A.A., Becker, R.O., Bachman, C.H., 1967. Dielectric determination of bound water of bone. Phys. Med. Biol. 12 (3), 367–378. https://doi.org/10.1088/0031-9155/12/3/309.

Marshall, D., Johnell, O., Wedel, H., 1996. Meta-analysis of how well measures of bone mineral density predict occurrence of osteoporotic fractures. BMJ 312 (7041), 1254–1259. https://doi.org/10.1136/bmj.312.7041.1254.

Masic, A., Bertinetti, L., Schuetz, R., Chang, S.W., Metzger, T.H., Buehler, M.J., Fratzl, P., 2015. Osmotic pressure induced tensile forces in tendon collagen. Nat. Commun. 6, 5942. https://doi.org/10.1038/ncomms6942.

Mastrogiacomo, S., Dou, W., Jansen, J.A., Walboomers, X.F., 2019. Magnetic resonance imaging of hard tissues and hard tissue engineered bio-substitutes. Mol. Imaging Biol. 21 (6), 1003–1019. https://doi.org/10.1007/s11307-019-01345-2.

McNally, E.A., Schwarcz, H.P., Botton, G.A., Arsenault, A.L., 2012. A model for the ultrastructure of bone based on electron microscopy of ion-milled sections. PLoS One 7 (1), e29258. https://doi.org/10.1371/journal.pone.0029258.

McNerny, E.M.B., Buening, D.T., Aref, M.W., Chen, N.X., Moe, S.M., Allen, M.R., 2019. Time course of rapid bone loss and cortical porosity formation observed by longitudinal μCT in a rat model of CKD. Bone 125, 16–24. https://doi.org/10.1016/j.bone.2019.05.002.

Minami, M., Ikoma, K., Horii, M., Sukenari, T., Onishi, O., Fujiwara, H., Ogi, H., Itoh, K., Kubo, T., 2018. Usefulness of sweep imaging with fourier transform for evaluation of cortical bone in diabetic rats. J. Magn. Reson. Imaging 48 (2), 389–397. https://doi.org/10.1002/jmri.25955.

Mitome, J., Yamamoto, H., Saito, M., Yokoyama, K., Marumo, K., Hosoya, T., 2011. Nonenzymatic cross-linking pentosidine increase in bone collagen and are associated with disorders of bone mineralization in dialysis patients. Calcif. Tissue Int. 88 (6), 521–529. https://doi.org/10.1007/s00223-011-9488-y.

Mkukuma, L.D., Skakle, J.M., Gibson, I.R., Imrie, C.T., Aspden, R.M., Hukins, D.W., 2004. Effect of the proportion of organic material in bone on thermal decomposition of bone mineral: an investigation of a variety of bones from different species using thermogravimetric analysis coupled to mass spectrometry, high-temperature X-ray diffraction, and Fourier transform infrared spectroscopy. Calcif. Tissue Int. 75 (4), 321–328. https://doi.org/10.1007/s00223-004-0199-5.

Mkukuma, L.D., Imrie, C.T., Skakle, J.M., Hukins, D.W., Aspden, R.M., 2005. Thermal stability and structure of cancellous bone mineral from the femoral head of patients with osteoarthritis or osteoporosis. Ann. Rheum. Dis. 64 (2), 222–225. https://doi.org/10.1136/ard.2004.021329.

Monteiro, D.A., Dole, N.S., Campos, J.L., Kaya, S., Schurman, C.A., Belair, C.D., Alliston, T., 2021. Fluid shear stress generates a unique signaling response by activating multiple TGFbeta family type I receptors in osteocytes. FASEB J 35 (3), e21263. https://doi.org/10.1096/fj.202001998R.

Mooney, S.D., Klein, T.E., 2002. Structural models of osteogenesis imperfecta-associated variants in the COL1A1 gene. Mol. Cell. Proteomics 1 (11), 868–875. https://doi.org/10.1074/mcp.m200064-mcp200.

Moore, E.R., Ryu, H.S., Zhu, Y.X., Jacobs, C.R., 2018. Adenylyl cyclases and TRPV4 mediate Ca(2+)/cAMP dynamics to enhance fluid flow-induced osteogenesis in osteocytes. J Mol Biochem 7, 48–59.

Morrell, A.E., Brown, G.N., Robinson, S.T., Sattler, R.L., Baik, A.D., Zhen, G., Cao, X., Bonewald, L.F., Jin, W., Kam, L.C., Guo, X.E., 2018. Mechanically induced Ca(2+) oscillations in osteocytes release extracellular vesicles and enhance bone formation. Bone Res. 6, 6. https://doi.org/10.1038/s41413-018-0007-x.

Morris, M.D., Mandair, G.S., 2011. Raman assessment of bone quality. Clin. Orthop. Relat. Res. 469 (8), 2160–2169. https://doi.org/10.1007/s11999-010-1692-y.

Mroue, K., MacKinnon, N., Xu, J., Zhu, P., McNerny, E., Kohn, D.H., Morris, M.D., Ramamoorthy, A., 2012. High-resolution structural insights into bone: a solid-state NMR relaxation study utilizing paramagnetic doping. J. Phys. Chem. B 116 (38), 11656–11661. https://doi.org/10.1021/jp307935g.

Mroue, K.H., Nishiyama, Y., Kumar Pandey, M., Gong, B., McNerny, E., Kohn, D.H., Morris, M.D., Ramamoorthy, A., 2015. Proton-detected solid-state NMR spectroscopy of bone with ultrafast magic angle spinning. Sci Rep 5, 11991. https://doi.org/10.1038/srep11991.

Mroue, K.H., Xu, J., Zhu, P., Morris, M.D., Ramamoorthy, A., 2016. Selective detection and complete identification of triglycerides in cortical bone by high-resolution (1)H MAS NMR spectroscopy. Phys. Chem. Chem. Phys. 18 (28), 18687–18691. https://doi.org/10.1039/c6cp03506j.

Murray, D.T., Das, N., Cross, T.A., 2013. Solid state NMR strategy for characterizing native membrane protein structures. Acc. Chem. Res. 46 (9), 2172–2181. https://doi.org/10.1021/ar3003442.

Nalla, R.K., Balooch, M., Ager 3rd, J.W., Kruzic, J.J., Kinney, J.H., Ritchie, R.O., 2005. Effects of polar solvents on the fracture resistance of dentin: role of water hydration. Acta Biomater. 1 (1), 31–43. https://doi.org/10.1016/j.actbio.2004.08.002.

Neuman, W.F., Neuman, M.W., 1958. The chemical dynamics of bone mineral.

Newman, C.L., Moe, S.M., Chen, N.X., Hammond, M.A., Wallace, J.M., Nyman, J.S., Allen, M.R., 2014. Cortical bone mechanical properties are altered in an animal model of progressive chronic kidney disease. PLoS One 9 (6), e99262. https://doi.org/10.1371/journal.pone.0099262.

Ni, Q., Nyman, J.S., Wang, X., Santos, A.D.L., Nicolella, D.P., 2007. Assessment of water distribution changes in human cortical bone by nuclear magnetic resonance. Meas. Sci. Technol. 18, 715–723.

Nickolas, T.L., Leonard, M.B., Shane, E., 2008. Chronic kidney disease and bone fracture: a growing concern. Kidney Int. 74 (6), 721–731. https://doi.org/10.1038/ki.2008.264.

Nikel, O., Laurencin, D., Bonhomme, C., Sroga, G.E., Besdo, S., Lorenz, A., Vashishth, D., 2012. Solid state NMR investigation of intact human bone quality: balancing issues and insight into the structure at the organic-mineral interface. J. Phys. Chem. C Nanomater. Interfaces 116 (10), 6320–6331. https://doi.org/10.1021/jp2125312.

Nyman, J.S., Roy, A., Shen, X., Acuna, R.L., Tyler, J.H., Wang, X., 2006. The influence of water removal on the strength and toughness of cortical bone. J. Biomech. 39 (5), 931–938. https://doi.org/10.1016/j.jbiomech.2005.01.012.

Nyman, J.S., Ni, Q., Nicolella, D.P., Wang, X., 2008. Measurements of mobile and bound water by nuclear magnetic resonance correlate with mechanical properties of bone. Bone 42 (1), 193–199. https://doi.org/10.1016/j.bone.2007.09.049.

Nyman, J.S., Gorochow, L.E., Adam Horch, R., Uppuganti, S., Zein-Sabatto, A., Manhard, M.K., Does, M.D., 2013. Partial removal of pore and loosely bound water by low-energy drying decreases cortical bone toughness in young and old donors. J. Mech. Behav. Biomed. Mater. 22, 136–145. https://doi.org/10.1016/j.jmbbm.2012.08.013.

Nyman, J.S., Uppuganti, S., Unal, M., Leverant, C.J., Adabala, S., Granke, M., Voziyan, P., Does, M.D., 2019. Manipulating the amount and structure of the organic matrix affects the water compartments of human cortical bone. JBMR Plus 3 (6), e10135. https://doi.org/10.1002/jbm4.10135.

Ong, H.H., Wright, A.C., Wehrli, F.W., 2012. Deuterium nuclear magnetic resonance unambiguously quantifies pore and collagen-bound water in cortical bone. J. Bone Miner. Res. 27 (12), 2573–2581. https://doi.org/10.1002/jbmr.1709.

Park, E.Y., Lee, D., Lee, C., Kim, C., 2020. Non-ionizing label-free photoacoustic imaging of bones. IEEE Access 8, 160915–160920. https://doi.org/10.1109/ACCESS.2020.3020559.

Pathak, S., Swadener, J.G., Kalidindi, S.R., Courtland, H.W., Jepsen, K.J., Goldman, H. M., 2011. Measuring the dynamic mechanical response of hydrated mouse bone by nanoindentation. J. Mech. Behav. Biomed. Mater. 4 (1), 34–43. https://doi.org/10.1016/j.jmbbm.2010.09.002.

Penel, G., Delfosse, C., Descamps, M., Leroy, G., 2005. Composition of bone and apatitic biomaterials as revealed by intravital Raman microspectroscopy. Bone 36 (5), 893–901. https://doi.org/10.1016/j.bone.2005.02.012.

Powell, K.M., Skaggs, C., Pulliam, A., Berman, A., Allen, M.R., Wallace, J.M., 2019. Zoledronate and raloxifene combination therapy enhances material and mechanical properties of diseased mouse bone. Bone 127, 199–206. https://doi.org/10.1016/j.bone.2019.06.018.

Powell, K.M., Brown, A.P., Skaggs, C.G., Pulliam, A.N., Berman, A.G., Deosthale, P., Plotkin, L.I., Allen, M.R., Williams, D.R., Wallace, J.M., 2020. 6'-methoxy raloxifene-analog enhances mouse bone properties with reduced estrogen receptor binding. Bone Rep. 12, 100246. https://doi.org/10.1016/j.bonr.2020.100246.

Privalov, P.L., 1958. State and role of water in biological systems. Biofizika 3 (6), 738–743.

Rai, R.K., Sinha, N., 2011. Dehydration-induced structural changes in the collagen-hydroxyapatite Interface in bone by high-resolution solid-state NMR spectroscopy. J. Phys. Chem. C 115 (29), 14219–14227. https://doi.org/10.1021/jp2025768.

Rai, R.K., Barbhuyan, T., Singh, C., Mittal, M., Khan, M.P., Sinha, N., Chattopadhyay, N., 2013. Total water, phosphorus relaxation and inter-atomic organic to inorganic interface are new determinants of trabecular bone integrity. PLoS One 8 (12), e83478. https://doi.org/10.1371/journal.pone.0083478.

Rai, R.K., Singh, C., Sinha, N., 2015. Predominant role of water in native collagen assembly inside the bone matrix. J. Phys. Chem. B 119 (1), 201–211. https://doi.org/10.1021/jp511288g.

Rajapakse, C.S., Bashoor-Zadeh, M., Li, C., Sun, W., Wright, A.C., Wehrli, F.W., 2015. Volumetric cortical bone porosity assessment with MR imaging: validation and clinical feasibility. Radiology 276 (2), 526–535. https://doi.org/10.1148/radiol.15141850.

Rajapakse, C.S., Padalkar, M.V., Yang, H.J., Ispiryan, M., Pleshko, N., 2017. Non-destructive NIR spectral imaging assessment of bone water: comparison to MRI measurements. Bone 103, 116–124. https://doi.org/10.1016/j.bone.2017.06.015.

Reichert, D., Pascui, O., Bonagamba, T.J., Arnold, K., Huster, D., de Azevedo, E.R., 2004. A solid-state NMR study of the fast and slow dynamics of collagen fibrils at varying hydration levels. Magn. Reson. Chem. 42 (2), 276–284. https://doi.org/10.1002/mrc.1334.

Rey, J.R., Cervino, E.V., Rentero, M.L., Crespo, E.C., Alvaro, A.O., Casillas, M., 2009. Raloxifene: mechanism of action, effects on bone tissue, and applicability in clinical traumatology practice. Open Orthop. J. 3, 14–21. https://doi.org/10.2174/1874325000903010014.

Reznikov, N., Bilton, M., Lari, L., Stevens, M.M., Kroger, R., 2018. Fractal-like hierarchical organization of bone begins at the nanoscale. Science 360 (6388). https://doi.org/10.1126/science.aao2189.

Rho, J.Y., Pharr, G.M., 1999. Effects of drying on the mechanical properties of bovine femur measured by nanoindentation. J ,Mater. Sci. Mater. Med. 10 (8), 485–488. https://doi.org/10.1023/a:1008901109705.

Riggs, B.L., Melton 3rd, L.J., 2002. Bone turnover matters: the raloxifene treatment paradox of dramatic decreases in vertebral fractures without commensurate increases in bone density. J. Bone Miner. Res. 17 (1), 11–14. https://doi.org/10.1359/jbmr.2002.17.1.11.

Ritchie, R.O., Nalla, R.K., Kruzic, J.J., Ager III, J.W., Balooch, G., Kinney, J.H., 2006. Fracture and ageing in bone: toughness and structural characterization. Strain 42 (4), 225–232. https://doi.org/10.1111/j.1475-1305.2006.00282.x.

Robinson, W., 1931. Free and bound water determinations by the heat of fusion of ice method. J Biol Chem (92), 699–709.

Robinson, R.A., 1952. An electron-microscopic study of the crystalline inorganic component of bone and its relationship to the organic matrix. J Bone Joint Surg Am 34-A (2), 389–435 passim.

Robson, M.D., Bydder, G.M., 2006. Clinical ultrashort echo time imaging of bone and other connective tissues. NMR Biomed. 19 (7), 765–780. https://doi.org/10.1002/nbm.1100.

Rokidi, S., Paschalis, E.P., Klaushofer, K., Vennin, S., Desyatova, A., Turner, J.A., Watson, P., Lappe, J., Akhter, M.P., Recker, R.R., 2019. Organic matrix quality discriminates between age- and BMD-matched fracturing versus non-fracturing post-menopausal women: a pilot study. Bone 127, 207–214. https://doi.org/10.1016/j.bone.2019.06.017.

Rokidi, S., Andrade, V.F.C., Borba, V., Shane, E., Cohen, A., Zwerina, J., Paschalis, E.P., Moreira, C.A., 2020. Bone tissue material composition is compromised in premenopausal women with type 2 diabetes. Bone 141, 115634. https://doi.org/10.1016/j.bone.2020.115634.

Samuel, J., Sinha, D., Zhao, J.C., Wang, X., 2014. Water residing in small ultrastructural spaces plays a critical role in the mechanical behavior of bone. Bone 59, 199–206. https://doi.org/10.1016/j.bone.2013.11.018.

Samuel, J., Park, J.S., Almer, J., Wang, X., 2016. Effect of water on nanomechanics of bone is different between tension and compression. J. Mech. Behav. Biomed. Mater. 57, 128–138. https://doi.org/10.1016/j.jmbbm.2015.12.001.

Samuel, J., Park, J.S., Almer, J., Wang, X., 2016. Effect of water on nanomechanics of bone is different between tension and compression. J. Mech. Behav. Biomed. Mater. 57, 128–138. https://doi.org/10.1016/j.jmbbm.2015.12.001.

Sarkar, S., Mitlak, B.H., Wong, M., Stock, J.L., Black, D.M., Harper, K.D., 2002. Relationships between bone mineral density and incident vertebral fracture risk with raloxifene therapy. J. Bone Miner. Res. 17 (1), 1–10. https://doi.org/10.1359/jbmr.2002.17.1.1.

Sedlin, E.D., Hirsch, C., 1966. Factors affecting the determination of the physical properties of femoral cortical bone. Acta Orthop. Scand. 37 (1), 29–48. https://doi.org/10.3109/17453676608989401.

Seeman, E., 2017. Overview of bone microstructure, and treatment of bone fragility in chronic kidney disease. Nephrology (Carlton) 22 (Suppl. 2), 34–35. https://doi.org/10.1111/nep.13024.

Seifert, A.C., Wehrli, F.W., 2016. Solid-state quantitative (1)H and (31)P MRI of cortical bone in humans. Curr. Osteoporos. Rep. 14 (3), 77–86. https://doi.org/10.1007/s11914-016-0307-2.

Seifert, A.C., Wehrli, S.L., Wehrli, F.W., 2015. Bi-component T2 * analysis of bound and pore bone water fractions fails at high field strengths. NMR Biomed. 28 (7), 861–872. https://doi.org/10.1002/nbm.3305.

Shanas, N., Querido, W., Oswald, J., Jepsen, K., Carter, E., Raggio, C., Pleshko, N., 2021. EXPRESS: infrared spectroscopy-determined bone compositional changes associated with anti-resorptive treatment of the oim/oim mouse model of osteogenesis imperfecta. Appl. Spectrosc. https://doi.org/10.1177/00037028211055477, 37028211055477.

Sheer, R.L., Barron, R.L., Sudharshan, L., Pasquale, M.K., 2020. Validated prediction of imminent risk of fracture for older adults. Am J Manag Care 26 (3), e91–e97. https://doi.org/10.37765/ajmc.2020.42641.

Singh, C., Rai, R.K., Sinha, N., 2013. Experimental aspect of solid-state nuclear magnetic resonance studies of biomaterials such as bones. Solid State Nucl. Magn. Reson. 54, 18–25. https://doi.org/10.1016/j.ssnmr.2013.05.003.

Singh, C., Rai, R.K., Aussenac, F., Sinha, N., 2014. Direct evidence of imino acid-aromatic interactions in native collagen protein by DNP-enhanced solid-state NMR

spectroscopy. J. Phys. Chem. Lett. 5 (22), 4044–4048. https://doi.org/10.1021/jz502081j.
Siriwanarangsun, P., Statum, S., Biswas, R., Bae, W.C., Chung, C.B., 2016. Ultrashort time to echo magnetic resonance techniques for the musculoskeletal system. Quant Imaging Med Surg 6 (6), 731–743. https://doi.org/10.21037/qims.2016.12.06.
Sukenari, T., Horii, M., Ikoma, K., Kido, M., Hayashi, S., Hara, Y., Yamasaki, T., Matsuda, K., Kawata, M., Kubo, T., 2015. Cortical bone water changes in ovariectomized rats during the early postoperative period: objective evaluation using sweep imaging with fourier transform. J. Magn. Reson. Imaging 42 (1), 128–135. https://doi.org/10.1002/jmri.24765.
Surowiec, R.K., Battle, L.F., Ward, F.S., Schlecht, S.H., Khoury, B.M., Robbins, C., Wojtys, E.M., Caird, M.S., Kozloff, K.M., 2020. A xenograft model to evaluate the bone forming effects of sclerostin antibody in human bone derived from pediatric osteogenesis imperfecta patients. Bone 130, 115118. https://doi.org/10.1016/j.bone.2019.115118.
Surowiec, R.K., Ram, S., Idiyatullin, D., Goulet, R., Schlecht, S.H., Galban, C.J., Kozloff, K.M., 2021. In vivo quantitative imaging biomarkers of bone quality and mineral density using multi-band-SWIFT magnetic resonance imaging. Bone 143, 115615. https://doi.org/10.1016/j.bone.2020.115615.
Tastad, C.A., Kohler, R., Wallace, J.M., 2021. Limited impacts of thermoneutral housing on bone morphology and mechanical properties in growing female mice exposed to external loading and raloxifene treatment. Bone 146, 115889. https://doi.org/10.1016/j.bone.2021.115889.
Timmins, P.A., Wall, J.C., 1977. Bone water. Calcif. Tissue Res. 23 (1), 1–5. https://doi.org/10.1007/BF02012759.
Tiwari, N., Rai, R., Sinha, N., 2020. Water-lipid interactions in native bone by high-resolution solid-state NMR spectroscopy. Solid State Nucl. Magn. Reson. 107, 101666 https://doi.org/10.1016/j.ssnmr.2020.101666.
Trebacz, H., Wojtowicz, K., 2005. Thermal stabilization of collagen molecules in bone tissue. Int. J. Biol. Macromol. 37 (5), 257–262. https://doi.org/10.1016/j.ijbiomac.2005.04.007.
Tremollieres, F.A., Pouilles, J.M., Drewniak, N., Laparra, J., Ribot, C.A., Dargent-Molina, P., 2010. Fracture risk prediction using BMD and clinical risk factors in early postmenopausal women: sensitivity of the WHO FRAX tool. J. Bone Miner. Res. 25 (5), 1002–1009. https://doi.org/10.1002/jbmr.12.
Unal, M., Akkus, O., 2015. Raman spectral classification of mineral- and collagen-bound water's associations to elastic and post-yield mechanical properties of cortical bone. Bone 81, 315–326. https://doi.org/10.1016/j.bone.2015.07.024.
Unal, M., Yang, S., Akkus, O., 2014. Molecular spectroscopic identification of the water compartments in bone. Bone 67, 228–236. https://doi.org/10.1016/j.bone.2014.07.021.
Uppuganti, S., Granke, M., Makowski, A.J., Does, M.D., Nyman, J.S., 2016. Age-related changes in the fracture resistance of male fischer F344 rat bone. Bone 83, 220–232. https://doi.org/10.1016/j.bone.2015.11.009.
Van Dijk, F.S., Sillence, D.O., 2014. Osteogenesis imperfecta: clinical diagnosis, nomenclature and severity assessment. Am. J. Med. Genet. A 164a (6), 1470–1481. https://doi.org/10.1002/ajmg.a.36545.
Vennin, S., Desyatova, A., Turner, J.A., Watson, P.A., Lappe, J.M., Recker, R.R., Akhter, M.P., 2017. Intrinsic material property differences in bone tissue from patients suffering low-trauma osteoporotic fractures, compared to matched non-fracturing women. Bone 97, 233–242. https://doi.org/10.1016/j.bone.2017.01.031.
Vesper, E.O., Hammond, M.A., Allen, M.R., Wallace, J.M., 2017. Even with rehydration, preservation in ethanol influences the mechanical properties of bone and how bone responds to experimental manipulation. Bone 97, 49–53. https://doi.org/10.1016/j.bone.2017.01.001.
Vestergaard, P., 2007. Discrepancies in bone mineral density and fracture risk in patients with type 1 and type 2 diabetes–a meta-analysis. Osteoporos. Int. 18 (4), 427–444. https://doi.org/10.1007/s00198-006-0253-4.
Von Euw, S., Chan-Chang, T.-H.-C., Paquis, C., Haye, B., Pehau-Arnaudet, G., Babonneau, F., Azaïs, T., Nassif, N., 2018. Organization of Bone Mineral: the role of mineral-water interactions. Geosciences 8 (12), 466.
Vyalikh, A., Elschner, C., Schulz, M.C., Mai, R., Scheler, U., 2017. Early stages of biomineral formation—a solid-state NMR investigation of the mandibles of minipigs. Magnetochemistry 3 (4), 39.
Wang, L., 2018. Solute transport in the bone lacunar-canalicular system (LCS). Curr. Osteoporos. Rep. 16 (1), 32–41. https://doi.org/10.1007/s11914-018-0414-3.
Wang, X., Ni, Q., 2003. Determination of cortical bone porosity and pore size distribution using a low field pulsed NMR approach. J. Orthop. Res. 21 (2), 312–319. https://doi.org/10.1016/s0736-0266(02)00157-2.
Wang, F., Zhao, Y., 2011. Slip boundary conditions based on molecular kinetic theory: the critical shear stress and the energy dissipation at the liquid–solid interface. Soft Matter 7 (18), 8628–8634. https://doi.org/10.1039/C1SM05543G.
Wang, Y., Von Euw, S., Fernandes, F.M., Cassaignon, S., Selmane, M., Laurent, G., Pehau-Arnaudet, G., Coelho, C., Bonhomme-Coury, L., Giraud-Guille, M.M., Babonneau, F., Azais, T., Nassif, N., 2013. Water-mediated structuring of bone apatite. Nat. Mater. 12 (12), 1144–1153. https://doi.org/10.1038/nmat3787.
Wang, X., Xu, H., Huang, Y., Gu, S., Jiang, J.X., 2016. Coupling effect of water and proteoglycans on the in situ toughness of bone. J. Bone Miner. Res. 31 (5), 1026–1029. https://doi.org/10.1002/jbmr.2774.
Wang, X., Hua, R., Ahsan, A., Ni, Q., Huang, Y., Gu, S., Jiang, J.X., 2018. Age-related deterioration of bone toughness is related to diminishing amount of matrix glycosaminoglycans (Gags). JBMR Plus 2 (3), 164–173. https://doi.org/10.1002/jbm4.10030.
Wang, G., Xu, W., Zhang, J., Tang, T., Chen, J., Fan, C., 2021. Induction of bone remodeling by raloxifene-doped iron oxide functionalized with hydroxyapatite to accelerate fracture healing. J. Biomed. Nanotechnol. 17 (5), 932–941. https://doi.org/10.1166/jbn.2021.3068.
Wang, S., Suhaimi, H., Mabrouk, M., Georgiadou, S., Ward, J.P., Das, D.B., 2021. Effects of scaffold pore morphologies on glucose transport limitations in hollow fibre membrane bioreactor for bone tissue engineering: experiments and numerical modelling. Membranes (Basel) 11 (4). https://doi.org/10.3390/membranes11040257.
Wehrli, F.W., Fernandez-Seara, M.A., 2005. Nuclear magnetic resonance studies of bone water. Ann. Biomed. Eng. 33 (1), 79–86. https://doi.org/10.1007/s10439-005-8965-8.
Weiger, M., Pruessmann, K.P., Hennel, F., 2011. MRI with zero echo time: hard versus sweep pulse excitation. Magn. Reson. Med. 66 (2), 379–389. https://doi.org/10.1002/mrm.22799.
Weiger, M., Pruessmann, K.P., Bracher, A.K., Köhler, S., Lehmann, V., Wolfram, U., Hennel, F., Rasche, V., 2012. High-resolution ZTE imaging of human teeth. NMR Biomed. 25 (10), 1144–1151. https://doi.org/10.1002/nbm.2783.
Welborn, V.V., 2021. Environment-controlled water adsorption at hydroxyapatite/collagen interfaces. Phys. Chem. Chem. Phys. 23 (25), 13789–13796. https://doi.org/10.1039/D1CP01028J.
Williams, H.J., Davies, A.M., 2006. The effect of X-rays on bone: a pictorial review. Eur. Radiol. 16 (3), 619–633. https://doi.org/10.1007/s00330-005-0010-7.
Wilson, E.E., Awonusi, A., Morris, M.D., Kohn, D.H., Tecklenburg, M.M., Beck, L.W., 2005. Highly ordered interstitial water observed in bone by nuclear magnetic resonance. J. Bone Miner. Res. 20 (4), 625–634. https://doi.org/10.1359/JBMR.041217.
Wilson, E.E., Awonusi, A., Morris, M.D., Kohn, D.H., Tecklenburg, M.M., Beck, L.W., 2006. Three structural roles for water in bone observed by solid-state NMR. Biophys. J. 90 (10), 3722–3731. https://doi.org/10.1529/biophysj.105.070243.
Xia, J., Yao, J., Wang, L.V., 2014. Photoacoustic tomography: principles and advances. Electromagn. Waves (Camb.) 147, 1–22. https://doi.org/10.2528/pier14032303.
Xu, Z., Li, C., Wang, L.V., 2010. Photoacoustic tomography of water in phantoms and tissue. J. Biomed. Opt. 15 (3), 036019. https://doi.org/10.1117/1.3443793.
Yamada, H., Evans, F.G., 1970. Strength of biological materials. Williams & Wilkins, Baltimore.
Yamashita, J., Furman, B.R., Rawls, H.R., Wang, X., Agrawal, C.M., 2001. The use of dynamic mechanical analysis to assess the viscoelastic properties of human cortical bone. J. Biomed. Mater. Res. 58 (1), 47–53. https://doi.org/10.1002/1097-4636(2001)58:1<47::aid-jbm70>3.0.co;2-u.
Yan, J., Daga, A., Kumar, R., Mecholsky, J.J., 2008. Fracture toughness and work of fracture of hydrated, dehydrated, and ashed bovine bone. J. Biomech. 41 (9), 1929–1936. https://doi.org/10.1016/j.jbiomech.2008.03.037.
Yoder, C.H., Pasteris, J.D., Worcester, K.N., Schermerhorn, D.V., 2012. Structural water in carbonated hydroxylapatite and fluorapatite: confirmation by solid state (2)H NMR. Calcif. Tissue Int. 90 (1), 60–67. https://doi.org/10.1007/s00223-011-9542-9.
Zhao, X., Song, H.K., Seifert, A.C., Li, C., Wehrli, F.W., 2017. Feasibility of assessing bone matrix and mineral properties in vivo by combined solid-state 1H and 31P MRI. PLOS ONE 12 (3), e0173995. https://doi.org/10.1371/journal.pone.0173995.
Zhu, P., Xu, J., Sahar, N., Morris, M.D., Kohn, D.H., Ramamoorthy, A., 2009. Time-resolved dehydration-induced structural changes in an intact bovine cortical bone revealed by solid-state NMR spectroscopy. J. Am. Chem. Soc. 131 (47), 17064–17065. https://doi.org/10.1021/ja9081028.
Zhu, P., Xu, J., Sahar, N., Morris, M.D., Kohn, D.H., Ramamoorthy, A., 2009. Time-resolved dehydration-induced structural changes in an intact bovine cortical bone revealed by solid-state NMR spectroscopy. J. Am. Chem. Soc. 131 (47), 17064–17065. https://doi.org/10.1021/ja9081028.